Noise-induced spatiotemporal patterns in a bistable reaction-diffusion system: Photoelectron emission microscopy experiments and modeling of the CO oxidation reaction on Ir(111)

Patrick Hoffmann,[1] Stefan Wehner,[2,*] Dieter Schmeisser,[1] Helmut R. Brand,[3] and Jürgen Küppers[2,4]
[1]*Angewandte Physik II, Brandenburgische Technische Universität Cottbus, 03013 Cottbus, Germany*
[2]*Experimentalphysik III, Universität Bayreuth, 95440 Bayreuth, Germany*
[3]*Theoretische Physik III, Universität Bayreuth, 95440 Bayreuth, Germany*
[4]*Max-Planck-Institut für Plasmaphysik (EURATOM Association), 85748 Garching, Germany*
(Received 24 January 2006; published 23 May 2006)

We use photoelectron emission microscopy (PEEM) measurements to study the spatiotemporal patterns obtained for the CO oxidation reaction on Ir(111) as a function of the noise strength we superpose on the CO and the oxygen fractions of the constant total reactant gas flux. The investigations are focused on the bistable regime this reaction displays including its monostable vicinity. Simultaneously we analyze numerically the underlying reaction-diffusion (RD) equations in two spatial dimensions. For intrinsic and/or small strength of the external noise we find transitions from the locally stable to the globally stable branch via slow nucleation and growth of islands of the globally stable state: oxygen or CO, respectively. With increasing noise strength the number of islands as well as their growth rate increases. These phenomena are very well reproduced by numerical calculations of the RD model. For sufficiently large noise strength we observe bursts from CO rich to oxygen rich and back as well as switching between the two states. While such phenomena are also obtained from the model calculations, their experimentally observed spatial scales were not satisfactorily reproduced using the same approach as for the lower noise strengths.

DOI: 10.1103/PhysRevE.73.056123 PACS number(s): 82.40.Ck, 82.40.Np, 05.40.−a

I. INTRODUCTION

The formation of spatial patterns and their time evolution in systems which exhibit chemically reacting species has attracted significant experimental and theoretical research. For several decades, the system studied most frequently was the Belousov-Zhabotinsky reaction [1], which can be demonstrated in a Petri dish. A complete theoretical description of this reaction is, however, hampered by the fact that several reactants and intermediates are involved in the pattern forming processes which makes its system of reaction-diffusion (RD) differential equations (RDEs) rather complex. In addition, it depends on the time scales of interest how many species and intermediate steps enter the associated RD system [2].

A much simpler set of two RDEs for only two reacting species u and v as proposed by FitzHugh and Nagumo (FHN) and before that in a different context by Bonhoeffer and van der Pol [3] reads

$$u_t = u_{xx} + f(u) - v, \tag{1}$$

$$v_t = \delta v_{xx} + \sigma u - \gamma v \tag{2}$$

with δ, σ, γ positive and $f(u)=u(1-u)(u-a)$ or similar expressions. It is seen that in these FHN equations v acts as an inhibitor on u and v, u acts as an activator on v, and the dynamics of u is driven by a nonlinear force in u. Originally the FHN equations were derived [4,5] to describe the propagation of the action potential in the nerve fibers of the squid giant axon, for which a large body of work had been carried out before by Hodgkin and Huxley. This set of RDEs and variations thereof were analyzed in many studies [6–9] and were found to provide a rich variety of concentration patterns and reaction fronts, e.g., spirals [10] and waves [11]. Almost all of these features reflect the fact that the system considered is excitable.

Surfaces are ideal templates for experimental studies of reaction-diffusion systems since the two-dimensional character of these reactions allows comparison with two-dimensional model studies which are much less numerically complex than their three-dimensional counterparts. If a simple surface reaction is studied which involves only two reactant and one product species without participation of intermediates, modeling of the experiment through an appropriate set of kinetic equations is further simplified. In addition, a surface and the gas phase in contact with it can be prepared and maintained in a well defined manner. Through repetitive cleaning reproducible surface conditions can be installed prior to performing experiments. In a continuously pumped reactor the flux of the reactants to the surface can be varied rather precisely by simple means and the reaction rate can be continuously monitored via mass spectroscopy. In contrast, with experiments performed using reactive solutions in a Petri dish, the small aspect ratio of the experimental system makes the installation of continuously fed reactor conditions a nontrivial task. The biggest advantage of surface reactions, however, is that the availability of photoelectron emission microscopy (PEEM) allows us to monitor the spatial distribution of the reactant species *in situ* during reaction on a scale down to a few μm, provided that the work function contrast between patches of these species on the surface is sufficiently large. PEEM was employed in the spectacular experiments on rate oscillations in the CO-oxidation reaction on Pt(100) and Pt(110) surfaces [12–15] and more recently to study spatiotemporal effects in this reaction on Pt(111)

*Electronic address: stefan.wehner@uni-bayreuth.de

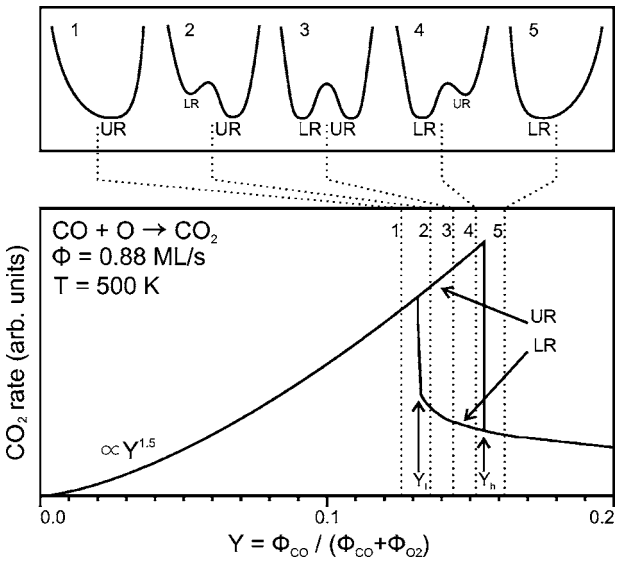

FIG. 1. Lower part: schematic representation of the CO_2 rate hysteresis measured at 500 K in the CO oxidation reaction on Ir(111) surfaces as a function of the CO fraction Y in the reactant CO+oxygen gas flux. The numbers refer to the potential diagram shown in the upper part. Upper part: potential curves for the stable and bistable regimes of the rate hysteresis shown in the lower part.

[16] and other reactions on Rh(111) surfaces [17,18].

Any experiment is subjected to noise, may it be created internally and not under control of the experimenter, or externally, due to insufficient regulation of an experimental parameter, for example, temperature, pressure, input flux of reactants, and similar quantities. Intuitively one expects that noise imposed intentionally on those quantities would significantly affect the patterns evolving in a reaction-diffusion system and that at a sufficiently high noise level the patterns would vanish altogether and get replaced by features without any spatial structure.

In order to investigate the consequences of externally applied noise on a reaction-diffusion system we have recently performed experiments and calculations of the CO oxidation reaction rate on Ir(111) surfaces. As on other structurally stable (no adsorption-induced-reconstruction) coinage metal surfaces, Pt(111) [16,19] and Pd(111) nanocrystals [20,21], this reaction exhibits a kinetic phase transition in the CO_2 rate as a function of the CO fraction Y in the CO+oxygen input gas flux [22]. For easy orientation the CO_2 rate measured at Ir(111) at 500 K is schematically shown in the lower panel of Fig. 1 [23]. If Y is increased from zero the rate increases in a nonlinear fashion. At these Y values, with $Y=0$ as initial condition, the surface exhibits a high O coverage and a high CO_2 rate. If Y passes a specific value Y_h, the CO_2 rate drops sharply and remains at that low level upon further increasing Y, indicative of a surface which is predominantly covered by CO. Upon decreasing Y the CO_2 rate stays at a low level even when Y_h is passed and recovers to the high CO_2 rate level only if Y has reached the value Y_l. Apparently, between Y_l and Y_h the system exhibits bistability: if Y is located between Y_l and Y_h a high or low CO_2 rate will be measured, depending on whether Y was approached from $Y=0$ (100% oxygen in the input gas flux) or $Y=1$ (100% CO in the input gas flux). This bistability causes a rate hysteresis with upper (high CO_2 rate, UR) and lower (low CO_2 rate, LR) rate branches. As shown earlier [23], by appropriately pulsing the input gas flux from O rich to CO rich and vice versa, one can switch between the upper and lower rate branches in a rather predictable fashion and proper design of gas flux sequences allows one to place the system on any point of the two branches of the hysteresis, and even *temporarily* on unstable points in the CO_2 rate/Y diagram.

In a mean field approach [24,25], the CO_2 rate as a function of Y can be modeled by taking into account adsorption, desorption, reaction, and diffusion of CO and O. With $n_O(x,y,t)$, $n_{CO}(x,y,t)$, and $n_e(x,y,t)$ as space and time dependent concentrations of O covered, CO covered, and empty sites on the surface, the appropriate equations read [26,27]

$$\frac{\partial n_{CO}}{\partial t} = Y\Phi s_{CO} n_e/n_{Ir} - n_{CO}\nu_{deso}\exp(-E_{deso}/kT) - n_{CO}n_O\nu_{rea}\exp(-E_{rea}/kT) + D_{CO}\nabla^2 n_{CO}, \quad (3)$$

$$\frac{\partial n_O}{\partial t} = 2(1-Y)\Phi s_O (n_e/n_{Ir})^3 - n_{CO}n_O\nu_{rea}\exp(-E_{rea}/kT) + D_O\nabla^2 n_O, \quad (4)$$

$$\frac{dn_{CO_2}}{dt} = \Sigma(x,y) n_{CO} n_O \nu_{rea}\exp(-E_{rea}/kT), \quad (5)$$

$$n_{Ir} = n_e + n_{CO} + n_O \quad (6)$$

with Y as CO fraction in the total input gas flux Φ, s_{CO} and s_O as sticking coefficients of CO and oxygen, respectively, n_{Ir} as areal density of Ir atoms on the Ir(111) surface, ν_{deso} and E_{deso} as desorption frequency factor and energy of CO, ν_{rea} and E_{rea} as CO+O reaction frequency factor and activation energy, D_{CO}, D_O as diffusion coefficients, and T as temperature. In Eq. (4) desorption of oxygen is not considered since at the relevant temperature, $T=500$ K, its rate is negligible. The CO_2 rate dn_{CO_2}/dt in Eq. (5), which is only a function of time, is obtained by summation over all local contributions to the total rate, and Eq. (6) serves as normalization.

The parameters entering into Eqs. (3) and (4) are fairly well known from experiments and tabulated data. The CO_2 rate as a function of Y at $T=500$ K obtained from these equations matches very well the experimental data shown in Fig. 1, but is shifted a little on the Y scale [26,27]. Experiment and theory could be brought into better agreement by variation of parameters. However, since fitting of the model data to the experiment was and is not intended, even for the present work the parameter set already used in our previous papers [22,23,26–28,30] was used: $n_{Ir}=1.56\times10^{15}$ cm^{-2} $=1$ ML, $s_{CO}=1$, $\nu_{deso}=10^{13}$ s^{-1}, $E_{deso}=140$ kJ/mol, ν_{rea} $=10^5$ ML^{-1} s^{-1}, $E_{rea}=40$ kJ/mol, $s_O=0.11$ and where ML denotes monolayers. The total gas flux Φ used in these previous experiments was 1.37×10^{15} cm^{-2}.

A comparison of Eqs. (3) and (4) with the FHN equations from above illustrates significant similarities. The variables

n_{CO} and n_O act as inhibitors for the rates of these quantities and there is a nonlinearity affecting the rate of n_O. The activator component is hidden in the product rate which serves for supply of empty sites, i.e., increasing n_e. However, the FHN set of equations is not a "real world" reaction equation prototype since the product of u and v does not appear in the equations, as required if u and v react with each other. In contrast, the set of equations (3)–(6) exhibit terms which are proportional to both n_O and n_{CO}, simultaneously. This change leads to the feature that the present system is no longer excitable (compare Ref. [3] for a discussion of excitability in chemical reactions). The product terms qualify Eqs. (3)–(6), and similar sets of equations for Pt [25] and Pd [20] as test cases for mean-field descriptions of simple surface reactions. If these equations cannot only predict rates but also provide spatio-temporal behavior of $n_O(x,y,t)$ and $n_{CO}(x,y,t)$, which agrees with experimental data, the mean-field approach has qualified as a valuable description. We note that this "proof of principle" was already provided for the more complex case of oscillatory reactions [13,29].

The bistability phenomenon is often described by a double-well potential model as displayed in the upper panel of Fig. 1. Outside of the hysteresis region there is only one potential minimum, inside there are two. One of these latter potential minima is local, the other is global and through variation of reaction parameters, Y in the present case, the character of the minima can be changed. If Y is chosen close to the low-Y border of the hysteresis, the upper branch of the hysteresis represents the global minimum, if it is chosen close to the high-Y border of the hysteresis, the lower branch of the hysteresis represents the global minimum. Between these limiting cases exists an equipotential state, in which both minima are of equal depth. The double-well potential picture is only of descriptive nature and not strictly correct because the potential cannot be analytically written down, but it is very handy for illustration of the response of the reaction system to variations of external parameters. If, for example, the system is prepared on the lower branch of the hysteresis, close to its low-Y border, the system is located in a local minimum and the solutions of Eqs. (3)–(6) predict that it will stay there forever. A transition into the upper rate global minimum will only occur via application of means which kick the system over the barrier between the wells. The method of choice for achieving this is application of external noise. This can be rationalized in the following way. Through intrinsic noise of some origin there will be a narrow probability distribution of the states of the system with a maximum at the position of the local potential minimum. By application of external noise this distribution gets wider and at sufficiently large noise its wings will reach into the global potential minimum. If the noise amplitude is large enough, a transition of the system into the global potential minimum will occur.

Figure 2 illustrates two examples of experimental data which illustrate the action of noise in view of the double-minimum potential picture and are investigated with PEEM in the present paper. The data shown were collected during CO_2 rate measurements with external noise applied on Y and are taken from an earlier paper [26]. Figures 2(b)–2(d) show rates measured as a function of time at a location close to the left (Y_l) border of the hysteresis with superposition of Gaussian white noise (vide infra) components ΔY on Y. Figures 2(f)–2(h) show the analogue close to the right hysteresis border (Y_h). Initially, the system was prepared in the state of the local potential minimum at the selected Y, as indicated by an open dot in the icons shown on the right of the figures. The states of the respective global potential minimum are specified by full dots.

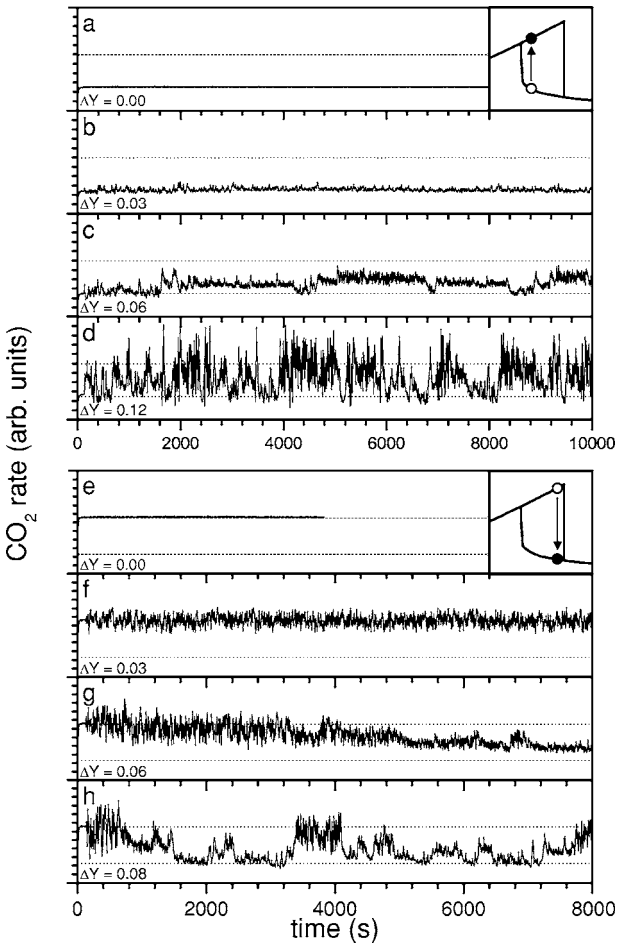

FIG. 2. CO_2 rates measured as a function of time for various noise amplitudes close to the left and right borders of the rate hysteresis. Data taken from Ref. [26].

Without application of external noise, the CO_2 rates are fairly constant. With application of noise on Y the rates also exhibit noise but in addition the system tends to approach the upper (lower) branch of the hysteresis when initially prepared on the lower (upper) branch. It is also apparent from Fig. 2 that at large noise levels the CO_2 rates exhibit substantial excursions, either for short time (rate bursts) or prolonged time (rate switches) [26,27]. A systematic scan of ΔY values at various Y revealed that outside of the hysteresis region, i.e., $Y<Y_l$ and $Y>Y_h$ noise on Y just produces a noisy CO_2 rate. For Y in the hysteresis region, $Y_l<Y<Y_h$, small noise amplitudes ΔY cause the rate to exhibit noise, but to stay on the upper (high rate) or lower (low rate) branches of the hysteresis at least for many hours. At medium noise amplitudes transitions between these branches occur, as illustrated in Fig. 2. The time required to complete

the transition gets smaller with increasing noise amplitude and Y values selected close to Y_l or Y_h: the bistability region shrinks with increasing noise on Y. Occasionally, the rate exhibits bursts. Application of large noise amplitudes leads to a loss of the bistability phenomenon and the CO_2 rate gets extremely noisy with rate bursts and rate switches occurring in a random, not oscillatory fashion.

Model calculations based on Eqs. (3)–(6) and including noise effects suggested that these phenomena are related to the spatiotemporal patterns evolving during reaction. The present study investigates these patterns using photoemission electron microscopy (PEEM) in a wide range of Y and ΔY values, not restricted to Y close to Y_l, as in our recent communication [30]. In addition, results are presented from solutions of the above reaction-diffusion equations for conditions close to these of the experiments.

II. EXPERIMENTAL METHODS

The experiments were performed in a UHV system located at the BTU Cottbus which was equipped with a PEEM, a quadrupole mass spectrometer, and a dedicated gas supply. The PEEM instrument (Focus/Omicron) is a high-stability device capable of long-term operation, tens of hours [31]. UV light was generated by a deuterium discharge lamp and focused via a lens system on the Ir(111) crystal. The work function contrast available in PEEM pictures was at the given photon energy sufficient to discriminate between clean (white), O covered (dark to black), and CO covered (light to dark grey) areas on the surface. This grey scale serves only for orientation in the experimental data presented below and will be addressed in the discussion section in more detail. The field of view of the PEEM was set at 310 μm, recorded by a CCD camera with 1404×1050 pixel resolution. The conformal mapping of the microscope was checked by recording the image of a Cu mesh with a repetition length of 12.5 μm and (7.5×7.5 μm^2) holes. It was also confirmed by PEEM images of this mesh that the current to heat the crystal did not distort the PEEM imaging. According to these checks it can be safely assumed that the recorded PEEM images (at the chosen 310 μm field of view) are neither affected by the instruments resolving power limitations nor by external field effects. Due to the limiting finite-size effects of work-function variations in PEEM, the actual resolution of the setup was about 3 μm. The Ir(111) crystal (9 mm diameter, 1.5 mm thickness, $<0.4°$ misorientation) was that specimen already used in the previous studies performed at the Universität Bayreuth [22,23,26–28]. In order to avoid stress from spotwelding-type crystal mounting it exhibits two spark-eroded grooves on opposite locations of its perimeter through which W heating/mounting wires were slid. As a consequence of this mounting technique, the crystal exposed a mirror finish throughout its surface. It was mounted on the lower end of a water-cooled x,y,z,Θ manipulator device. Its temperature was regulated via a type C thermocouple to a precision of <0.01 K. CO and oxygen were admitted via a doser tube directed at the crystal surface. In the gas supply of this tube the flows of oxygen and CO, supplied from pressurised high purity gas cylinders, were controlled by mass-flow controllers (MKS 200). After mixing of the gases, the backup total pressure on the back end of the doser was controlled by a capacitance manometer (MKS Baratron). The gas handling line was constructed by using only stainless-steel components and a dedicated turbomolecular pump based vacuum system. Sample cleaning was performed by Ar bombardment, annealing in oxygen at 1000 K, and flashing to 1500 K. The present experiments were performed at 500 K, as for many of our previous studies.

The combined flux of CO and oxygen was held constant throughout the present measurements, as was done previously. This flux was about 1.15 times the flux used previously, i.e., about 1.0 ML s^{-1} at BTU Cottbus instead of 0.88 ML s^{-1} at the Universität Bayreuth. As a consequence, the hysteresis, controlled by mass spectroscopy rate measurements, was shifted a bit towards lower Y values, between $Y_l=0.098$ and $Y_h=0.138$. Required Y values were set by programming the two mass flow controllers (MFCs) and random equally distributed ΔY components superimposed on Y were generated by randomly changing the MFC settings of the CO and oxygen gas flows around their mean values in 3 s intervals, but keeping the total flux constant. The combination of these flow changes, the doser tube conductivity, and the gas throughput of the vacuum system resulted in a distribution of Y values of the exposed gas flux which is well described by a Gaussian distribution with a variance of $(\Delta Y/2)^2$ around the mean Y [26,27]. The intrinsic noise on Y from the MFC characteristics was $\Delta Y=0.001$.

The experiments were performed in the following manner. The Ir(111) crystal was placed in front of the PEEM and PEEM images were recorded in 3 s intervals and stored. In the beginning of every experiment the Ir/CO/oxygen reaction system was set on a specific location in the CO_2 rate/Y diagram, see Fig. 1, by proper selection of a sequence of Y value settings without noise applied on these Y. The final Y of such a preparation determines the position of the system in the CO_2 rate/Y diagram, e.g., upper branch, close to right border of the hysteresis; lower branch, close to left border of the hysteresis. Note that these "jumps" to predefined locations on the CO_2 rate/Y diagram in a couple of several ten seconds requires sufficient control of the external parameter Y and a smoothly following reaction system. 300 s after the required CO_2 rate/Y location was installed following the procedure described above (it would stay there for many (>10) hours without application of noise on Y) a noise component ΔY was applied and the processes on the surface were recorded with PEEM as function of time, typically for several hours. The experiment was computer controlled and night/weekend runs were performed according to a predefined measurement task list.

III. THEORETICAL METHODS

The reaction-diffusion differential equations (RDEs), Eqs. (3)–(6), were solved previously [26,27] including the action of external Gaussian type noise on Y for one-dimensional (1D) and (2D) models. The essential characteristics of the experimental results of external noise effects on the CO_2 rates were reproduced in this work with both models and the

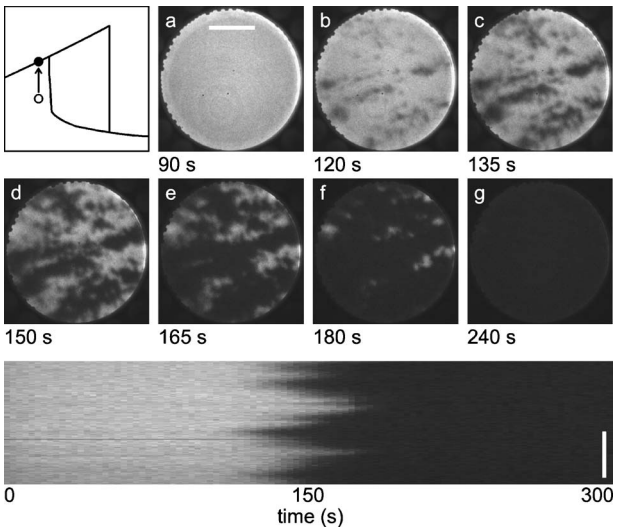

FIG. 3. PEEM sequence measured after initially preparing the system in an unstable point in the CO_2 rate/Y diagram at $Y=0.095$ without external noise applied, $\Delta Y=0$. The open dot in the icon shown in the upper left of the figure illustrates the location of the initial state. The arrow indicates to which state (black dot) the system moves. On the bottom a brightness time scan (x-t plot) is shown, taken along a 270 μm vertical pixel line in the center of the PEEM pictures. The white bars correspond to a length of 100 μm. The faint dark horizontal line in the x-t plot is due to a dead spot on the channelplate used for amplification. This dead spot can be seen in the PEEM pictures (a)–(c) of this figure. The irregular structures at the perimeter of the PEEM pictures originate from the metallic contact film on the channelplate boundary for high voltage connection.

calculations revealed interesting spatial effects which stimulated to perform the present study. In the present investigation, model calculations were performed along the following line. The set of parameters: energies, sticking factors, etc., was left unchanged as compared to our previous work. The total reactants gas flux Φ was adjusted to the value used in the present PEEM experiments. The calculations were done by iterating difference equations on (500×500) or (1000×1000) (x,y) grids with periodic boundary conditions. Time splitting between the adsorption-desorption-reaction and diffusion processes was implemented, as was done earlier. Space and time increments were set at dx, $dy=0.01$, $dt=0.01$. It was already confirmed in the earlier work [26,27] that other settings conforming with the convergence requirement [32] does not lead to other results.

Three aspects of the implementation of noise in the model calculations require special attention. If the Y variable in Eqs. (1) and (2) is changed to $Y+\Delta Y$, with ΔY a randomly changing quantity, these equations exhibit multiplicative as well as additive noise components [26,27]. These ΔY noise components were generated as Gaussian distributed white noise in space and time using random numbers calculated as proposed in the Numerical Recipes book [32].

The spatial component of the noise was constructed by application of the same noise level ΔY to the grid points (x,y) to $(x+n,y+n)$, with n a preselected number, $n=20$ used in the earlier work [26,27]. Since in the experiments the Y value of the CO+oxygen flux directed at the surface is spatially homogeneous, the randomness of Y in space must be delivered by the surface through variations of the local sticking coefficients. The value of n therefore is a noise averaging range which represents the unknown spatial extensions of these intrinsic local variations on the surface.

The temporal component of the noise was constructed by updating ΔY in time steps of 9 s, i.e., extrinsically. This 9 s interval differs from the experimentally selected 3 s interval. It (the 9 s interval) was selected for previous model calculations [26,27] in order to adjust the time scales on which experimental and model calculations CO_2 rate changes occur.

The noisy distribution of the Y values used in the calculations, i.e., the ΔY values superimposed on a mean Y value has a variance of $(\Delta Y)^2$ by construction [32]: The experimental ΔY value is expressed below by the half width of the equally distributed random number distribution used for programming of the MFC. The variance of the respective experimental Gaussian distributed noise on Y is given by $(\Delta Y/2)^2$. Accordingly, the experimental ΔY values given below are by a factor of 0.5 smaller than the ΔY values used for modeling.

IV. EXPERIMENTAL RESULTS

Prior to recording the PEEM sequences, the location of the rate hysteresis in the PEEM apparatus was determined with mass spectroscopy rate measurements, since this location is affected by the total CO+oxygen gas flux employed and the flux in the PEEM chamber was a factor of about 1.15 larger than that used in previous studies [26,27]. From these measurements the lower and upper edges, $Y_l=0.098$ and $Y_h=0.138$, of the rate hysteresis were obtained, see Fig. 1 for orientation.

The development of patterns as recorded by PEEM is shown in this section for five regimes of Y settings: (1) Y a little smaller than Y_l, (2) Y a little bigger than Y_l, (3) Y about halfway between Y_l and Y_h, (4) Y a little smaller than Y_h, and (5) Y a little bigger than Y_h. Comparing with Fig. 1 it is seen that with these settings locations just inside and outside of the hysteresis at its Y borders and in its center are probed. For easy orientation, each figure with PEEM sequences shown below displays in its upper left corner an icon of the hysteresis in which the initial and final states of the system are indicated by white and black dots, respectively, and an arrow which illustrates the path of the system. The patterns shown are the raw data delivered by a CCD camera, updated and stored every 3 s. The connection between the pattern brightness scale and the CO or oxygen coverage is not known. White bars are included in the figures to provide a 100 μm scale.

The experimental procedure to install an initial state of the surface consisted in directing a pure oxygen flux $(Y=0)$ at the surface for several minutes at 500 K. If the system was to be prepared in a low-rate state, a 60 s CO pulse $(Y=1)$ was applied. Subsequently, the required Y value was set and held there for 300 s without application of noise. Then the noise component ΔY was superimposed on Y during the remainder of the respective $(Y,\Delta Y)$ experiment.

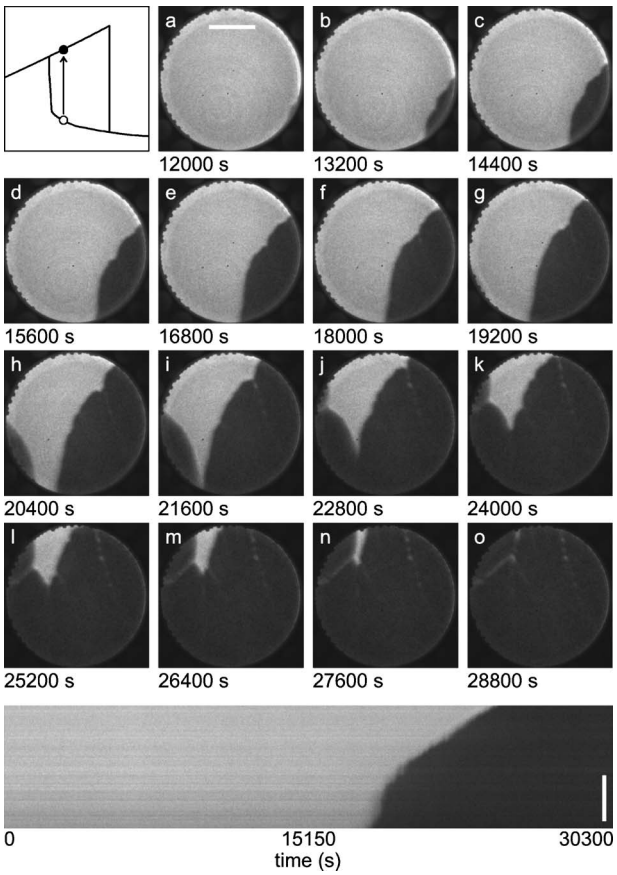

FIG. 4. PEEM sequence measured after initially preparing the system in a locally stable point on the lower branch of the hysteresis in the CO_2 rate/Y diagram close to the left border of the hysteresis $Y=0.11$ without external noise applied $\Delta Y=0$. Other details as for Fig. 3.

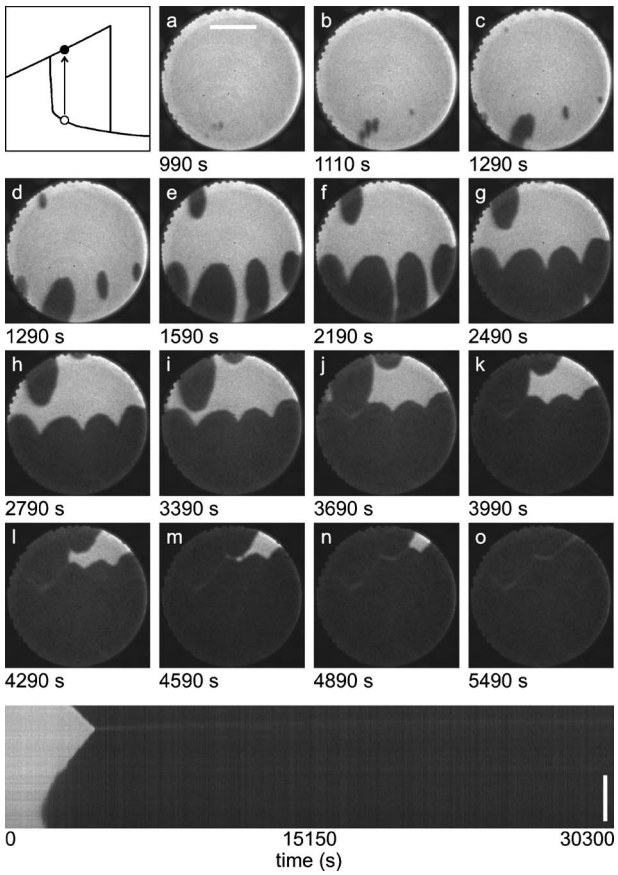

FIG. 5. PEEM sequence measured after initially preparing the system in a locally stable point on the lower branch of the hysteresis in the CO_2 rate/Y diagram close to the left border of the hysteresis $Y=0.11$ with external noise applied $\Delta Y=0.03$. Other details as for Fig. 3.

Figure 3 displays a PEEM sequence measured at a Y value smaller than Y_l without noise application and a low rate initial condition. Figure 3(a) shows the pattern obtained after installation of $Y=0.095$ at $t=0$ (subsequent to the 60 s CO pulse) and waiting for 90 s (between 0 and 90 s nothing happens). The pattern is grey, as expected for a CO covered surface. After 120 s [Fig. 3(b)] dark islands with fuzzy borders are seen which grow in density and size and collapse into a dark pattern of an oxygen covered surface after further 120 s [Fig. 3(g)].

On the bottom of Fig. 3 the time evolution of the brightness along a vertical pixel line in the center of the PEEM patterns, x-t plot for short, is shown. This representation is handy for visualizing the processes on the surface in a compact way. The transition from grey to dark at around 150 s reflects the transition seen in Figs. 3(b)–3(g) via the nucleation of islands, growth and collapse, even the islands fuzzy borders are apparent in the x-t plot. The CO covered surface state in which the reaction system was initially prepared at $t=0$, prior to recording of Fig. 3(a), is unstable. In a rather fast transition the system moves into the stable oxygen covered state on the upper branch of the hysteresis and remains there, refer to the icon in Fig. 3 and the potential diagram 1 in Fig. 1. The pattern development in Fig. 3 illustrates that this transition is mediated by the formation and fast growth of oxygen islands. The fuzziness of island borders apparent from Fig. 3 is an artifact. The integration time of the CCD camera was 2.86 s, by which contrast changes on the subscale necessarily lead to a fuzzy appearance of contrasts.

Figure 4 displays a PEEM sequence measured at $Y=0.11$, just inside of the hysteresis. Initially the system was prepared on the lower branch of the hysteresis. $Y=0.11$ was installed at $t=0$ s and beginning at $t=300$ s a noise of $\Delta Y=0.0$ (i.e., no external noise, only intrinsic noise in action) was applied. It is seen in the sequence that for several hours in the field of view of the microscope nothing happens: the pattern is grey, the surface remains CO covered. Then, Fig. 4(a), 12 000 s after the start of the experiment, the wall of an oxygen (black) island moves into the field of view from the lower right of the picture. Due to expansion of this oxygen island the wall moves slowly in a diagonal direction into the field of view, Figs. 4(b)–4(g). In Fig. 4(h) the occurrence of a second oxygen island is apparent on the lower left of the picture. The two islands merge in Fig. 4(i) and through steady wall motion seen in Figs. 4(j)–4(o) the merged islands eventually fill the entire field of view. 28 800 s (8 h) after start of the experiment the visible fraction of the surface is completely oxygen covered and the transition from the lower

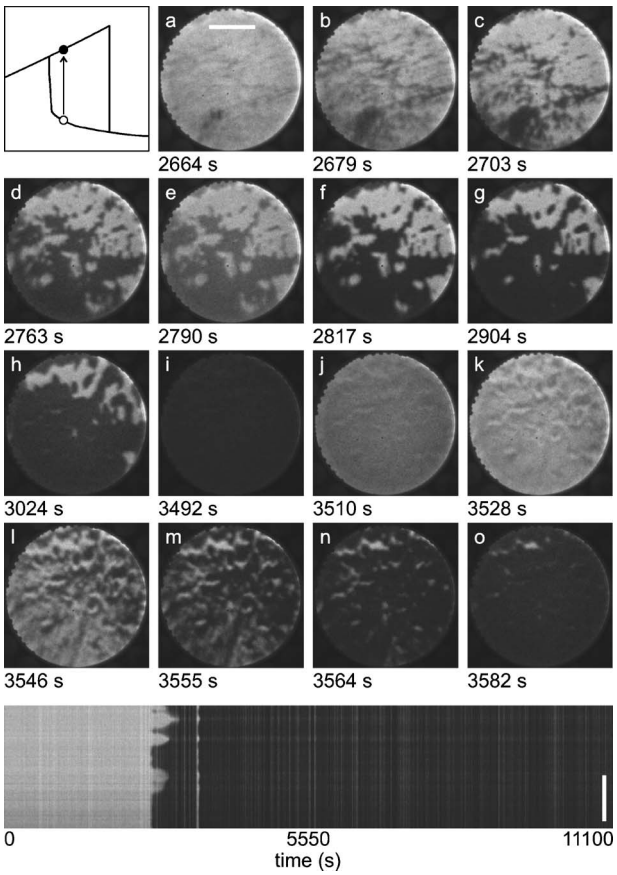

FIG. 6. PEEM sequence measured after initially preparing the system in a locally stable point on the lower branch of the hysteresis in the CO_2 rate/Y diagram close to the left border of the hysteresis $Y=0.11$ with external noise applied $\Delta Y=0.06$. Other details as for Fig. 3.

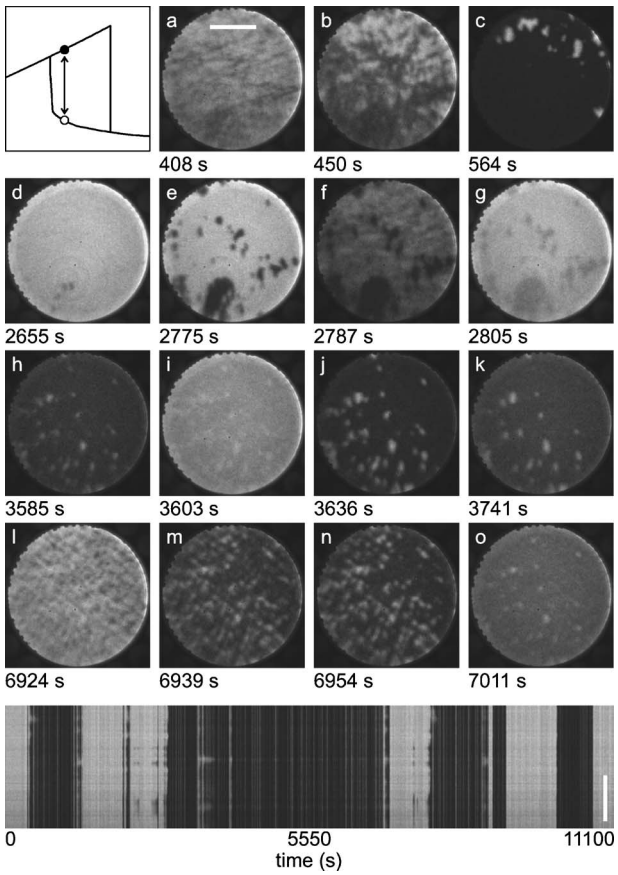

FIG. 7. PEEM sequence measured after initially preparing the system in a locally stable point on the lower branch of the hysteresis in the CO_2 rate/Y diagram close to the left border of the hysteresis $Y=0.11$ with external noise applied $\Delta Y=0.10$. Other details as for Fig. 3.

to the upper branch of the hysteresis is completed. This conclusion, however, applies only to the surface fraction seen by the PEEM. When the state of the surface is outside of the field of view of the microscope remains unknown.

In the bottom part of Fig. 4 the development of the brightness along the vertical pixel line of the PEEM patterns is shown. Clearly, the wall of an oxygen islands moves slowly across this line and in contrast to the x-t plot shown in Fig. 3, the grey-black boundary is rather sharp, in accordance with the minor brightness changes on a time scale of the CCD integration time of 2.86 s. From Fig. 4 it is immediately clear that the lower-to-upper branch transition has three characteristics: island wall motion determines the dynamics of the patterns, the patterns length scale is several 100 to 1000 μm, and their dynamics time scale is several 1000 s. These scales combined lead to extremely slow wall motion speeds.

A comment is in order concerning the reproducibility of the pattern evolutions measured with PEEM. In the usual sense the experiments were not reproducible. This is, however, required due to the randomness involved in performing these measurements. In reproducing experiments performed with the experiment design used for the data shown in Fig. 4, it could happen that after 10 h the system had not moved away from its initial location on the lower hysteresis branch: no island visible in the field of view. It could also happen that the low-to-high branch transition was completed in less than 8 h. With increasing noise amplitude ΔY these variations get smaller.

Figures 5 and 6 display the PEEM sequences measured at the same Y, $Y=0.11$, with larger ΔY values $\Delta Y=0.03$ and $\Delta Y=0.06$. The trends seen are larger ΔY increase the density of oxygen islands formed and accelerate the transition from the lower to the higher branch. The x-t plots illustrate this effect quite nicely. A special event is apparent from Figs. 6(i) and 6(j). The surface switches back from the "stable" oxygen covered state to the "unstable" CO covered state. This state switch is rather fast, within several ten s, and appears to occur homogeneously on the surface rather than through an island growth mechanism. The grey vertical line in the x-t plot illustrates that this switching event is clearly discernible in the time evolution of the PEEM pattern. We note the change in time scale going from Figs. 5 to 6.

At a noise amplitude of $\Delta Y=0.1$ a qualitative change is apparent. As seen in Fig. 7, the initial CO to oxygen covered surface (grey to black) transition occurs in several 100 s, Figs. 7(a)–7(c), however, in contrast to the pattern evolution seen in Figs. 4–6, the oxygen covered surface returns to a CO covered surface after 2655 s, Fig. 7(d), and switches

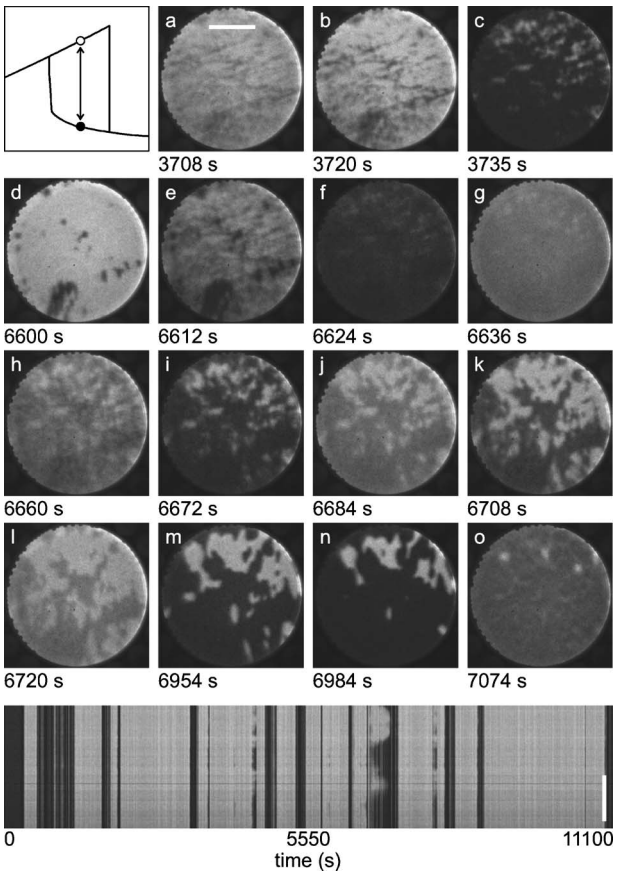

FIG. 8. PEEM sequence measured after initially preparing the system in a locally stable point on the upper branch of the hysteresis in the CO_2 rate/Y diagram close to the center of the hysteresis $Y=0.12$ with external noise applied $\Delta Y=0.12$. Other details as for Fig. 3.

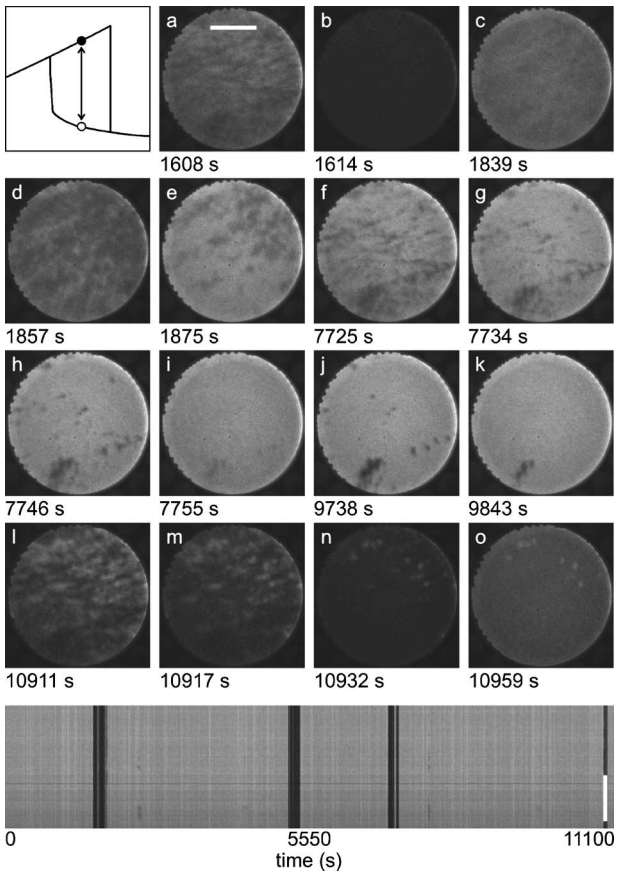

FIG. 9. PEEM sequence measured after initially preparing the system in a locally stable point on the lower branch of the hysteresis in the CO_2 rate/Y diagram close to the center of the hysteresis $Y=0.12$ with external noise applied $\Delta Y=0.10$. Other details as for Fig. 3.

back to an oxygen covered surface after 3585 s via island formation and growth, Figs. 7(e)–7(h). Then, after 3603 s it had returned back to CO covered in a short burst, Fig. 7(i), returns to oxygen covered at 3636 s, also in a burstlike fashion, Fig. 7(j), and back to CO covered, Fig. 7(l). From this state the surface returns to oxygen covered via island formation and growth to the oxygen covered state, Figs. 7(m)–7(o).

The essentials of this pattern sequence are available in compact form from the *x-t* plot shown at the bottom of Fig. 7. The grey-to-black (black-to-grey) changes monitor the CO-to-O (O-to-CO) transitions. If these transitions occur via vertically sharp brightness changes, the CO to oxygen (oxygen to CO) transitions are rather homogeneous and burstlike, as apparent from Figs. 7(f) and 7(g). The brightness changes in the *x-t* plot which exhibit irregular grey-black or black-grey borders indicate transitions between CO and O covered surfaces via island formation and growth, e.g., Figs. 7(j)–7(l). It is seen from the *x-t* plot in Fig. 7 that the abrupt brightness changes occur on shorter time scales than those which involve island formation processes. The experiment from Fig. 7 was ended after several hours and no projection can be made about its time evolution in the future, but the phenomenology seen suggests that these dark-grey and reverse transitions would occur even at later times.

In Fig. 8 the pattern evolution for $Y=0.12$, i.e., near the center of the hysteresis is shown, with the initial state prepared on the upper branch of the hysteresis and a noise amplitude of $\Delta Y=0.12$. This noise amplitude is significant. In the potential picture of Fig. 1 the system is close to the equipotential situation and the applied noise is at its reasonable limit: $\Delta Y=Y$. The pattern dynamics in Figs. 8(a)–8(o) displays transitions between the upper and lower branches of the hysteresis via various mechanisms, best seen in the *x-t* plot. Burstlike changes between a CO covered and O covered surface and vice versa occur as well as island formation and growth of either species in the background of the other. In agreement with the expectation drawn from Fig. 1, noise kicks the system back and forth between the potential wells.

The pattern development shown in Fig. 9 illustrates again an example with the setting $Y=0.12$, but smaller noise, $\Delta Y=0.10$, and initially prepared on the lower branch. The system switches between the states on the upper and lower branches, however, less often than in Fig. 8 because the noise amplitude is smaller. The brightness distribution in the *x-t* plot in Fig. 9 shows that the CO covered surface is preferred over the O covered surface. This suggests that the setting $Y=0.12$ does not really represent the equipotential situation but is slightly off.

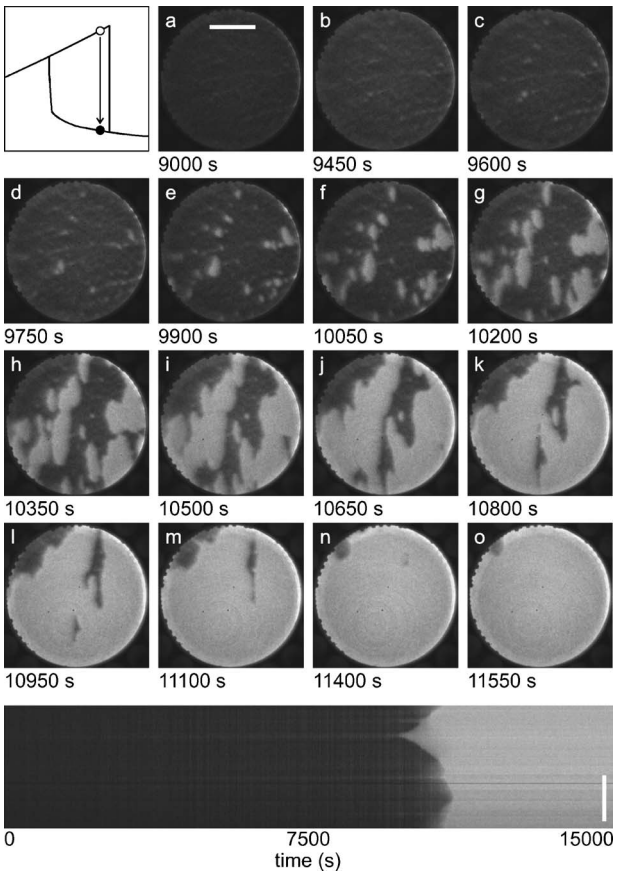

FIG. 10. PEEM sequence measured after initially preparing the system in a locally stable point on the upper branch of the hysteresis in the CO_2 rate/Y diagram close to the right border of the hysteresis $Y=0.13$ with external noise applied $\Delta Y=0.01$. Other details as for Fig. 3.

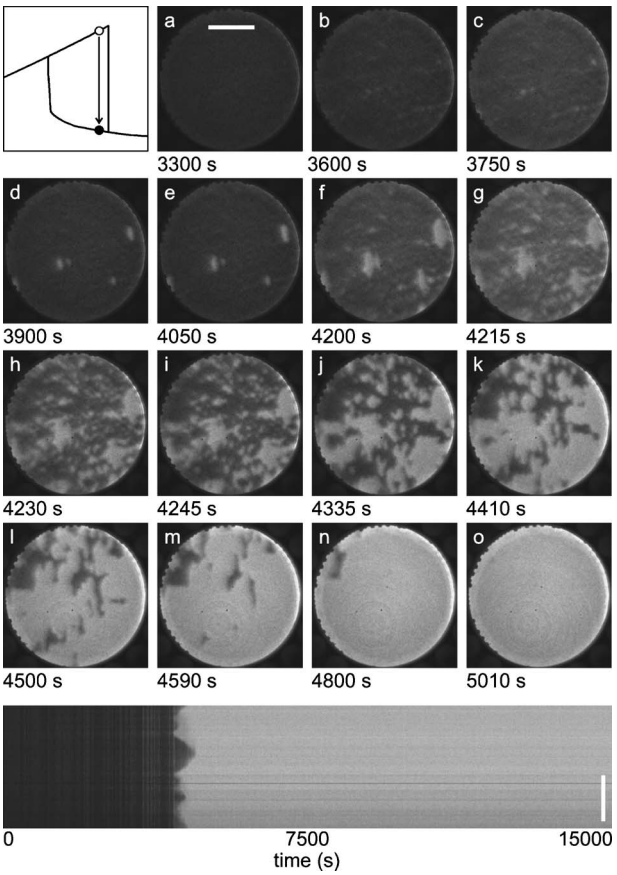

FIG. 11. PEEM sequence measured after initially preparing the system in a locally stable point on the upper branch of the hysteresis in the CO_2 rate/Y diagram close to the right border of the hysteresis $Y=0.13$ with external noise applied $\Delta Y=0.02$. Other details as for Fig. 3.

Figure 10 displays the pattern evolution measured close to the right border of the hysteresis, with small applied noise $Y=0.13$ and $\Delta Y=0.01$, and the system initially prepared on the upper branch of the hysteresis. For about 9000 s (2.5 h) nothing happens. Then a small CO island in the oxygen background occurs, Fig. 10(c). This island grows and on various other locations on the surface CO islands nucleate. Coalescence of the CO islands produces bizarre patterns, as those in Figs. 10(h)–10(j). Eventually, the surface in the field of view is covered with CO, about 12 000 s after start of the experiment. The *x-t* plot on the bottom of Fig. 10 illustrates that island formation and growth determines the dynamics of the system.

At increased noise amplitude $\Delta Y=0.02$ in Fig. 11, the high-to-low rate transition is faster and the density of formed CO islands is larger. After the CO covered state of the surface is reached, it stays there.

Increasing the noise amplitude to a high level $\Delta Y=0.1$ results in a significant acceleration of the transition to the low-rate branch with a CO covered surface, see the *x-t* plot in Fig. 12. However, the system tries to return to the oxygen rich surface around 4300 s. The first try seen in Figs. 12(a)–12(f) proceeds via island formation and growth and is not successful. The second try, a little later and apparent in Figs. 12(g)–12(i) is successful, but only temporarily. As the *x-t* plot and Figs. 12(i) and 12(j) show, the system returns to CO covered in a burst. At later times, around 9050 s the system temporarily switches form CO rich to oxygen rich.

At even higher noise amplitude these features get more prominent. Figure 13 collects PEEM pictures measured at $Y=0.13$ and $\Delta Y=0.12$. The *x-t* plot shown on the bottom of Fig. 13 suggest repeated tries of the system to make an excursion to the oxygen rich surface after it had moved within the first few 100 s to the CO rich surface. A comparison of the *x-t* plot with the selected PEEM pictures shows that these excursion might occur via island nucleation and growth or in a sudden switch. The PEEM sequence shown in Fig. 14 illustrates the systems response after it had been initially prepared in a state outside of the hysteresis at high oxygen coverage $Y=0.14$ and no external noise applied $\Delta Y=0$. The state is unstable and within a few 100 s the system moves to the CO rich state. The island borders in Figs. 14(d)–14(f) and the *x-t* plot dark-grey contrasts are fuzzy due to the same effect as noted for Fig. 3.

V. RESULTS OF MODEL CALCULATIONS

The set of PDEs, Eqs. (3)–(6) from above, was solved for various settings of Y and ΔY along the lines specified in Sec.

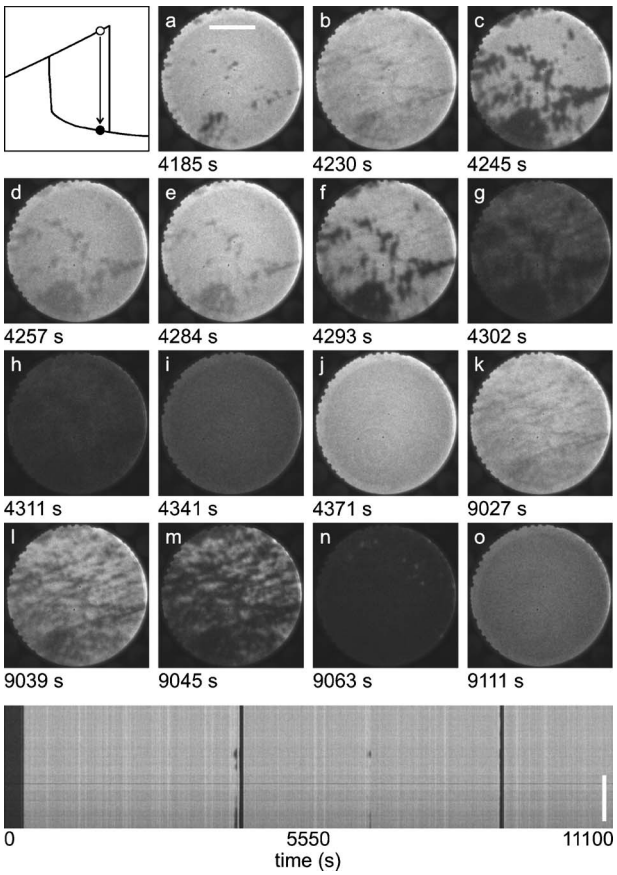

FIG. 12. PEEM sequence measured after initially preparing the system in a locally stable point on the upper branch of the hysteresis in the CO_2 rate/Y diagram close to the right border of the hysteresis $Y=0.13$ with external noise applied $\Delta Y=0.10$. Other details as for Fig. 3.

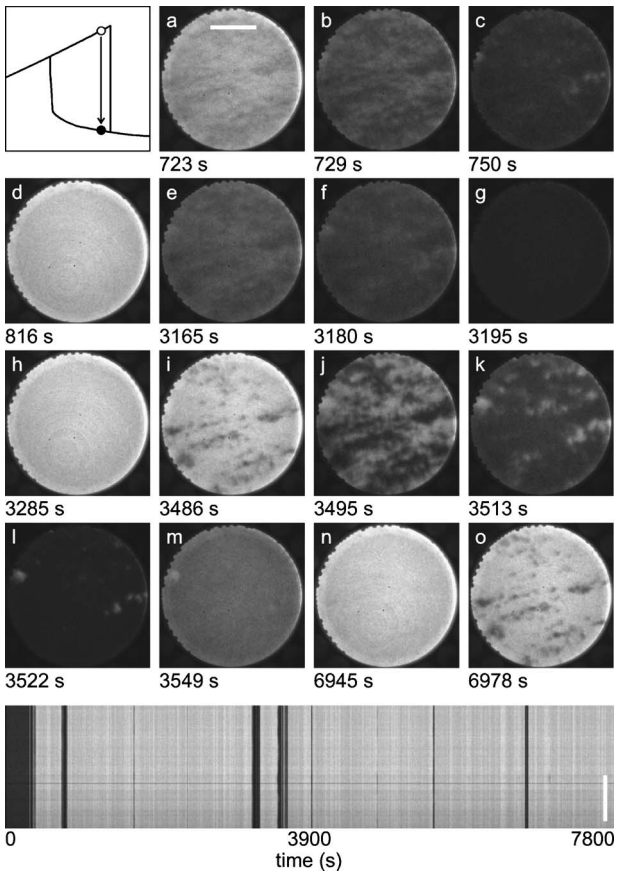

FIG. 13. PEEM sequence measured after initially preparing the system in a locally stable point on the upper branch of the hysteresis in the CO_2 rate/Y diagram close to the right border of the hysteresis $Y=0.13$ with external noise applied $\Delta Y=0.12$. Other details as for Fig. 3.

III. Since the parameters entering the PDE were fixed, there were two variables left: the size of the grid (500×500) or (1000×1000) and the spatial noise averaging range n. The choice of the grid size did not systematically affect the numerical results and data shown from the present calculations were obtained with a (500×500) grid.

As mentioned in Sec. III we use the same parameter set as in previous papers. Only the total reactant gas flux was adjusted to the value used for the PEEM experiments. This adjustment shifted the calculated Y hysteresis limits to $Y_l=0.068$ to $Y_h=0.119$, a bit downward from the earlier numerical values $Y_l=0.085$ to $Y_h=0.13$ [26]. whereas the measured values were $Y_l=0.098$ to $Y_h=0.138$. No efforts were undertaken to reduce these differences by parameter adjustments.

Figure 15 displays the pattern evolution calculated at $Y=0.076$, near the left border but inside of the hysteresis. The initial condition was set as CO covered, i.e., on the lower branch of the hysteresis. The noise was set at $\Delta Y=0.028$, and as values for spatial noise averaging $n=10$ (left panel in Fig. 15) and $n=20$ (right panel in Fig. 15) were employed. The grey scale used for this and subsequent figures which represent the results of model calculations was chosen in such a way that the transition from CO to O covered on a grid point (pixel) is represented by grey to black pixel settings, a choice which mimics the experimental situation. According to the initial condition, at $t=0$ the calculated pattern exhibited a grey appearance, CO covered.

In the left panel, $n=10$, the occurrence of a black (oxygen) island at the boundary of the model box is seen at $t=2\,415\,600$ time steps. Notice the consequence of periodic boundary conditions. At $t=2\,439\,000$ a second island developed. Through growth of these islands and their coalescence the box is eventually filled with black pixels. The evolution of the brightness along a vertical pixel line in the middle of the pattern shown in the x-t plot on the bottom of the figure is as expected. Notice that the x-t plot represents the brightness calculated on a vertical line in the center of the pictures shown in the left panel of Fig. 15. Accordingly, in the x-t plot the occurrence of the first dark structure is due to the small island seen at $t=2\,439\,000$.

In the right panel, $n=20$, the observed features are similar, only the density of black islands is bigger, many instead of one, and the time scale on which the transition grey to black (CO to oxygen covered) occurs is significantly shorter. The x-t plot illustrates the many-island pattern evolution process quite nicely.

In Fig. 16 calculated patterns are shown for the same initial condition, CO covered and an initially grey appear-

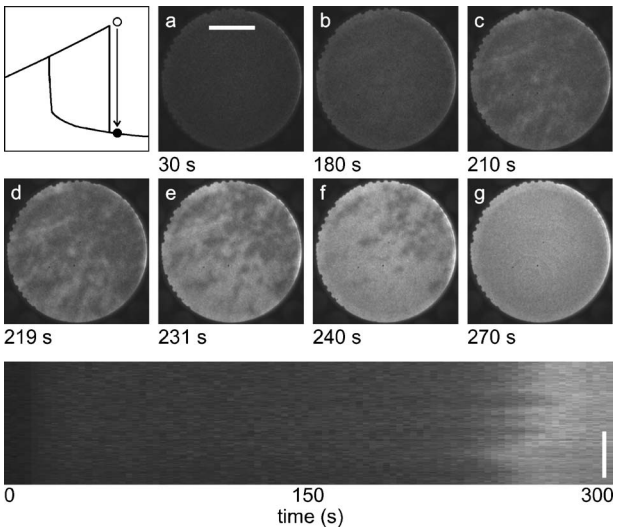

FIG. 14. PEEM sequence measured after initially preparing the system in an unstable point in the CO_2 rate/Y diagram at $Y=0.14$ without external noise applied, $\Delta Y=0$. Other details as for Fig. 3.

ance, and the same Y value $Y=0.076$, but for increased noise, $\Delta Y=0.040$. Values of n for spatial averaging were as for Fig. 15, $n=10$ and $n=20$. It is seen that due to the occurrence of many oxygen islands the patterns exhibit a granular structure, smaller granules at larger n. However, the consequences of the increase from $n=10$ to $n=20$ are less drastic as in Fig. 15, also apparent in the x-t plots on the bottom of Fig. 16.

Irrespective of the choice of n, the message of Figs. 15 and 16 is clear: A larger noise amplitude ΔY increases the density of islands formed and simultaneously decreases the time span needed for the transition from CO rich to O rich. These features were also observed in the experiments.

Figures 17 and 18 provide the patterns calculated at the right border of the hysteresis at $Y=0.111$, with noise amplitudes of $\Delta Y=0.016$ and $\Delta Y=0.030$. Initially the box (surface) was oxygen covered (black appearance). It is seen that irrespective of the noise level the system moves to the predominantly CO covered state and assumes a location on the low rate branch of the hysteresis. The transitions occur via CO island formation and growth. As also apparent from Figs. 15 and 16, larger n and larger ΔY values cause the density of islands to increase and the time required to complete the transition to decrease.

The x-t plots of the calculated pattern developments in Figs. 15–18 illustrate that the transitions from oxygen (CO) rich to CO (oxygen) rich are irreversible. Switches and bursts as seen in the experiment, e.g., in Fig. 7 for the transition from the lower rate branch to the upper rate branch, and in Figs. 12 and 13 for the transition from the upper rate branch to the lower rate branch, are not obtained from the model calculations. Inspection of many pattern development sequences calculated with n varied and large noise amplitudes revealed that the burst and switch phenomena occur, however, only on the scale of the space averaging dimension specified by n. Figure 19 displays x-t plots calculated for $Y=0.093$ (center of model hysteresis) with a CO covered surface as initial condition (lower branch of the hysteresis) and $\Delta Y=0.047$ using various spatial averaging ranges n

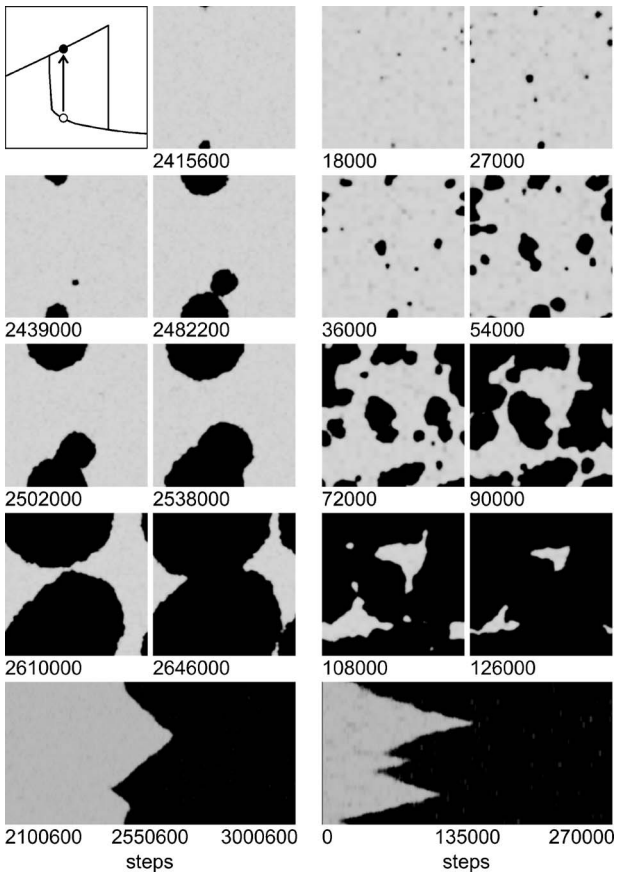

FIG. 15. Calculated coverage patterns and brightness time scans, oxygen dominated: black, CO dominated: grey, for the transition between a locally stable state on the lower and a globally stable state on the upper branch of the hysteresis. The icon in the top left illustrates the locations of these states. $Y=0.076$ and $\Delta Y=0.028$ were used. The left two columns correspond to a space averaging over $n=10$ cells, the two columns on the right to $n=20$ cells. The x-t plots shown on the bottom of this figure taken along a vertical top-to-bottom pixel line in the center of the calculated patterns.

$=10,20,50$, and 100 on a 500×500 cells grid. Each x-t plot shows vertical line scans over $5n$ cells, i.e., Fig. 19(a) over 50 cells, 19(b) over 100 cells, etc., and 19(d) over 500 cells which spans the full grid. At an averaging range of $n=10$ nothing happens, the system remains on the lower branch. At $n=20$, on a rare occasion, the system switches for a short time to the oxygen rich state and returns to the CO rich state. At $n=50$, switching occurs more frequently and for longer periods. This feature is even stronger expressed at $n=100$. It is, however, observed that the switching phenomena seen in Fig. 19 are restricted to the range of n. Unlike the experimental observations, the model calculations do not reveal that a large fraction of the surface is engaged in switching.

VI. DISCUSSION

The experimental results presented above illustrate that application of noise on the fractions of CO and oxygen in the constant total gas flux admitted to an Ir(111) surface leads to

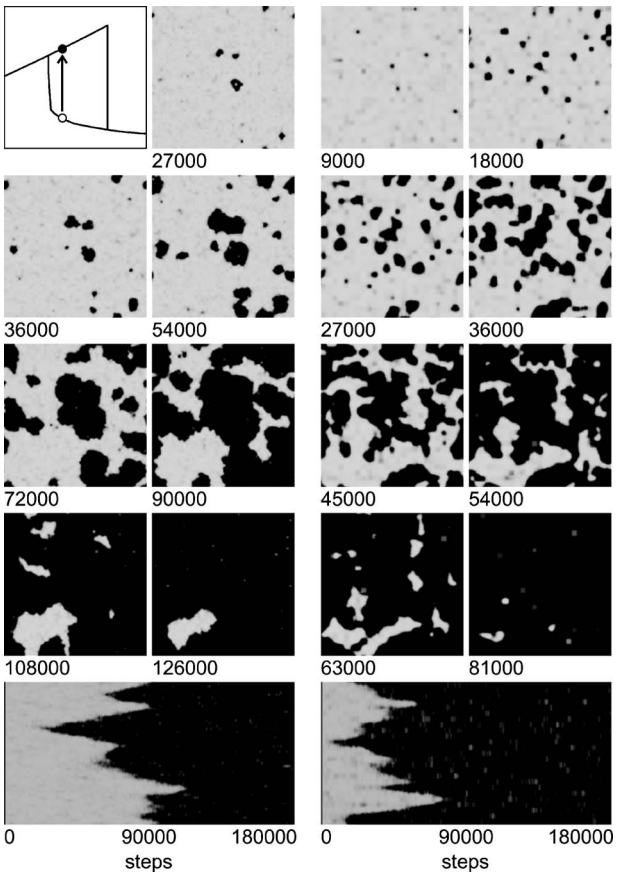

FIG. 16. As in Fig. 15, but with $Y=0.076$ and $\Delta Y=0.04$.

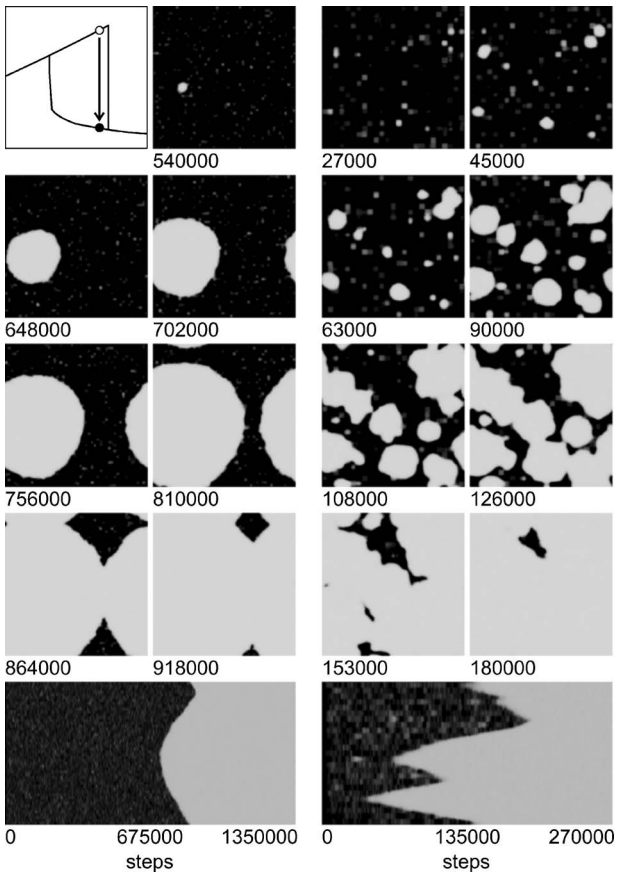

FIG. 17. As in Fig. 15, but with $Y=0.111$ and $\Delta Y=0.016$.

a significant modification of the spatiotemporal evolution of CO and oxygen island structures on the surface. The PEEM patterns shown in Figs. 4–7, measured at the left border of the rate hysteresis with increased noise amplitude, confirm the intuitive expectation that noise increases the areal density of islands and introduces an irregularity in the expression of these islands. The corresponding model data, Figs. 15 and 16 reproduce these features. The same characteristics were observed experimentally at the right border of the hysteresis, Figs. 10–13, and via modeling, Figs. 17 and 18.

Experiment and theory show that with increasing noise amplitude ΔY it becomes easier to nucleate new islands and therefore the density of islands increases when noise increases. The logic behind this effect stems from the higher probability to produce larger excursions in Y when the applied noise amplitude ΔY is increased.

Notwithstanding these agreements between experiment and theory, there are several issues to be considered more closely. In Fig. 4 it is seen that at the locations where the growing dark oxygen islands merge, narrow bright structures occur, best seen in the patterns which characterize the late state of the pattern development, Figs. 4(l)–4(o). Similar observations, however with significantly wider bright structures at the collision zones of reaction fronts were made in PEEM pictures of the pattern development at the hydrogen +oxygen [17] and NO+hydrogen reactions [18] on Rh(111) surfaces which were annealed in oxygen prior to reaction. As a tentative explanation the formation of a (sub)surface oxide was suggested. The present techniques do not allow to provide a better explanation, especially since the occurrence of these bright structures was not reproducible. Notice that in the PEEM pattern sequence shown in Fig. 5 the bright oxide structures are not seen on all collision zones of the reaction fronts. This phenomenon might be due to the fact that on a regular basis the Ir(111) surface was subjected to a high-temperature treatment in vacuo after an oxidation sequence between reaction cycles.

Due to its threefold symmetry, the Ir(111) surface does not exhibit a directional diffusion anisotropy and the shapes of the oxygen and CO islands in the background of the other species are expected to be circular, at least at small noise amplitudes. The oxygen islands in Fig. 4 are too large to judge whether they are circular since only a small fraction of their actual shape is seen in the PEEM pattern. The oxygen islands in Fig. 5 at larger size, later than Fig. 5(e), are definitely not circular but distorted elliptic with an aspect ratio of about 2–3. They are elongated in the vertical direction. This applies even more so to the shape of the CO islands seen in the PEEM sequence of Fig. 10. The patterns in Figs. 10(e)–10(h) display vertically elongated CO islands with an aspect ratio of 3 to 4. At later times the shapes of the islands cannot be specified any longer since they coalesce. The most plausible origin for the noncircular appearance of oxygen and CO islands are steps on the Ir(111) surface since stepped surfaces exhibit diffusional anisotropy: diffusion along the steps is faster than normal to them [33]. LEED pictures taken

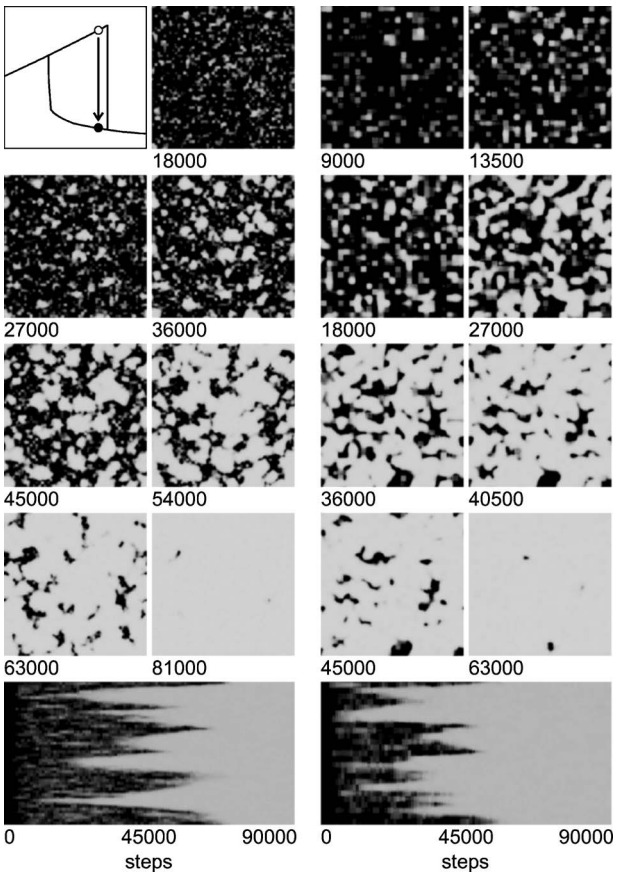

FIG. 18. As in Fig. 15, but with $Y=0.111$ and $\Delta Y=0.03$.

at the Ir(111) crystal in a different UHV system prior to the present PEEM study revealed that the surface did not exhibit regular steps. Spot splitting and regular spot intensity modulations were absent. The only indication of a not perfect surface were elongated LEED spots, indicative of steps, however, in a nonregular fashion. A study with an intentionally stepped surface might resolve that issue.

For the present investigation and comparison of the measured data with model calculation results it is essential that the pattern formation process occurs homogeneously and is not dominated by defects on the surface, i.e., it relies on surface heterogeneity. Inspection of Fig. 4 does not suggest heterogeneity effects in the oxygen island growth. In Fig. 5(b) on the lower right of the pattern two small oxygen islands are present in locations which are apparently prominent locations for oxygen island formation since in Fig. 6(a) and 6(c) fuzzy oxygen island structures are seen close to these locations, by which it is suggested that they act as nuclei for island growth. In Fig. 7(e) the same location is the origin of oxygen islands. A similar conclusion can be drawn from Figs. 5(c), 6(c), and 7(e) concerning a location at the 7 h position close to the boundary of the PEEM pictures: this location systematically occurs as a prominent center of an oxygen-rich structure.

Accordingly, there are heterogeneity effects, at least when oxygen islands grow on a CO covered surface. But these do not dominate the pattern forming processes and impose reproducible spatial pattern development features. For the growth of CO islands on an oxygen covered surface, Figs. 10–13 heterogeneity effects are not apparent.

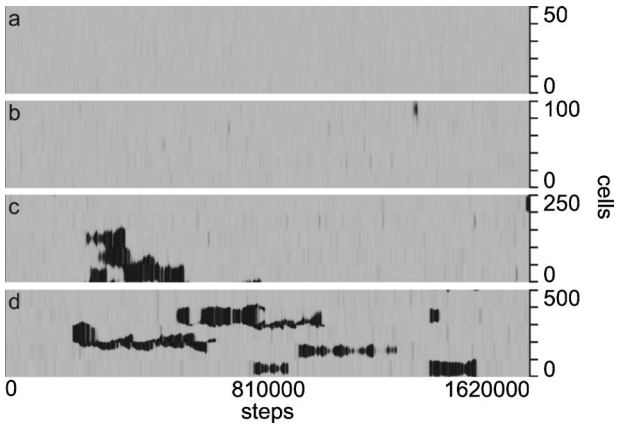

FIG. 19. *x-t* plots obtained by numerical simulation on a 500 $\times$ 500 grid for $Y=0.093$ and $\Delta Y=0.047$ using different spatial noise averaging ranges: (a) $n=10$, (b) $n=20$, (c) $n=50$, (d) $n=100$. Each plot displays a vertical scan line near the center of the patterns along $5n$ grid points.

The present PEEM measurements should fit into the picture developed earlier from rate measurements [26], i.e., there must be a connection between the rate data shown in Fig. 2 and the PEEM pictures shown in Figs. 4–13. This connection can be made in the following way. Dark regions in a PEEM picture are indicative of oxygen covered patches. These regions exhibit a high reactivity since adsorption of CO on these patches is not ruled out [Eq. (3)] and the oxygen+CO reaction on these patches is therefore favored. Conversely, light grey regions in the PEEM pictures are indicative of CO covered patches. Adsorption of oxygen on these patches is strongly reduced [Eq. (4)] and the oxygen +CO reaction rate is small on these fractions on the surface. The "darkness" of a PEEM picture is therefore proportional to the CO_2 rate obtained from the corresponding section of the surface.

In Fig. 20 the integrated darkness of the 270 μm diameter central section of the PEEM pictures for $Y=0.11$ (a)–(d) and $Y=0.13$ (e)–(h) is shown for various ΔY noise levels. These darkness data were calculated from the PEEM sequences collected for Figs. 5–7 and 11–13, and other data not shown explicitly. Since low darkness means grey, CO covered, and high darkness means black, oxygen covered, the vertical axis in this figure is proportional to the CO_2 rate and a direct comparison with the rate data shown in Fig. 2 should be possible.

The darkness curve for $\Delta Y=0.03$ in Fig. 20(a) is easy to interpret in view of Fig. 5 and its *x-t* plot. About 1000 s after start of the measurement with a CO covered surface as initial condition, the darkness starts to increase (oxygen islands develop). 4000 s later the entire field of view of the PEEM is dark and remains dark. At a noise amplitude of $\Delta Y=0.06$, Fig. 20(b), compare with Fig. 6, the transition from CO rich to oxygen rich starts at about 2500 s, several oxygen island grow and transform the CO rich to an oxygen rich surface. At about 3500 s a small peak to lower darkness indicates that temporarily fractions of the surface get CO covered. In the

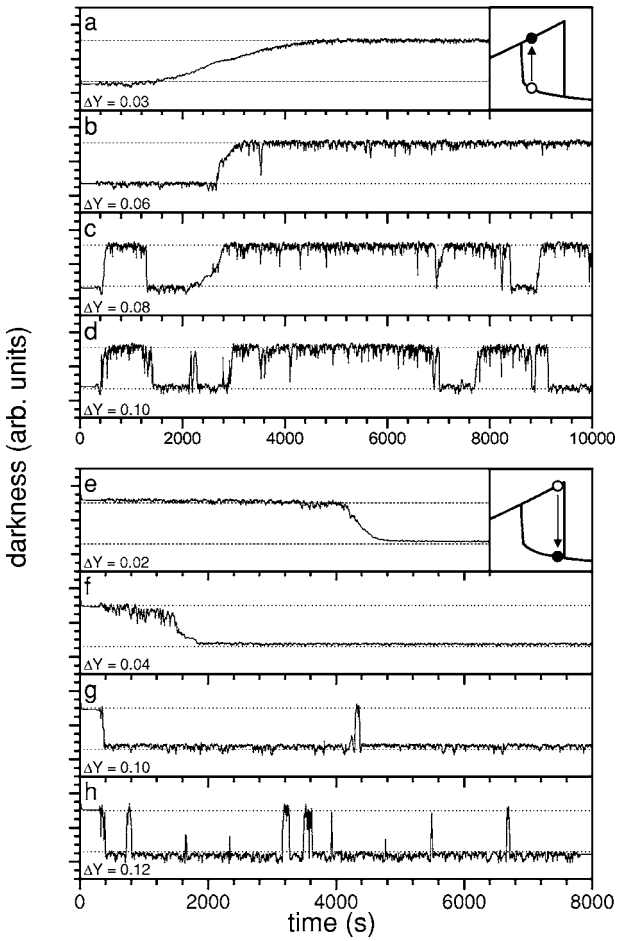

FIG. 20. Integrated darkness (the *y* scale displays brightness at small and darkness at large *y* values) determined from the PEEM patterns recorded during transitions between the upper and lower branches of the rate hysteresis at various ΔY values. (a) Corresponds to Fig. 5, (b) to Fig. 6, (d) to Fig. 7, (e) to Fig. 11, (g) to Fig. 12, and (h) to Fig. 13.

bottom of Fig. 6 this drop of darkness is apparent in the *x*-*t* plot. At a noise amplitude of $\Delta Y=0.08$, Fig. 20(c), the darkness assumes its maximum at about 400 s, stays there for 800 s, drops to low (grey), recovers to high (dark) in a slow transition around 2400 s, stays there with small excursions towards low for several 1000 s, makes a short excursion to low at 6800 s, recovers to high, stays at high until 8400 s, excurses to low and stays there for 600 s, returns to high. The darkness curve shown in Fig. 20(d) for $\Delta Y=0.1$ can be directly compared with the patterns and *x*-*t* plot in Fig. 7. The low-to-high and high-to-low darkness transitions and excursions in Fig. 19(d) just reflect the grey-to-dark and dark-to-grey changes in the *x*-*t* plot of Fig. 7. Accordingly, the darkness measure provides a compact representation of the spatiotemporal pattern development observed with PEEM and expressed in the *x*-*t* plots. Since from the above considerations the darkness is directly connected to the CO_2 rate, a connection between the PEEM patterns in Figs. 4–7, representative for the measurements at the left border of the hysteresis, and the CO_2 rate is possible.

Comparing the darkness curves in Fig. 20(e) to 20(h) with the PEEM patterns shown in Figs. 11–13, a similar conclusion can be drawn for the measurements performed on the right border of the hysteresis. In Fig. 20(e) (compare Fig. 11) it is seen that after a rather long high darkness period the system moves quietly to low darkness within less than 1000 s and stays there. At $\Delta Y=0.04$ the transition is faster and accompanied with a noisy expression of the darkness. At $\Delta Y=0.1$, Fig. 20(g) and corresponding PEEM patterns in Fig. 12, the transition from high to low darkness is even faster and around 4400 s an excursion to high darkness is apparent. In Fig. 20(h) (compare Fig. 13) excursions from low to high darkness occur more often, but the low darkness state qualifies as overall more stable.

With the darkness identified as a candidate quantity for a comparison of the rates and the PEEM patterns or *x*-*t* plots, a direct connection between Figs. 2 and 20 can be established. Upon comparing the time dependence of the CO_2 rates in Fig. 2 with the time dependence of the darkness in Fig. 20 one has, however, to consider that the rate data shown in Fig. 2 stem from the whole crystal area with 9 mm diameter, whereas the darkness data in Fig. 20 were obtained from a 270 μm diameter segment of this surface. Accordingly, the noisy rate with rate bursts and switches in Fig. 2(d) for $\Delta Y=0.12$ is a superposition of many uncorrelated darkness switches and bursts of the type seen in Fig. 20(d) for $\Delta Y=0.1$. The same applies to a comparison of Figs. 2(h), $\Delta Y=0.08$, and 20(h), $\Delta Y=0.12$. With decreasing noise amplitude the correlation between Figs. 2 and 20 is less obvious since the statistical sample of islands in the PEEM pattern gets smaller. However, having in mind that the randomness involved necessarily introduces differences between different measurements (data, Fig. 2 and data, Fig. 20) the correlation is strongly suggested for all panels in Figs. 2 and 20.

This statistics of islands is shown in the diagrams in Figs. 21(a)–21(h). The PEEM patterns used for construction of the darkness data in Fig. 21 were analyzed by a homemade pattern recognition program which counted the number of dark and grey structures with a closed boundary, irrespective of their shapes. It is clear from Fig. 21 that in total more than 20 000 PEEM patterns needed to be analyzed. The logarithmic scale used for display of the data illustrates that the number of structures in the PEEM patterns spans a considerable range.

The number of structures data in Fig. 21(a), $\Delta Y=0.03$ [compare Fig. 21(a) and the PEEM sequence in Fig. 5], illustrate that the transition from the lower branch to the upper branch of the hysteresis is accompanied by the formation of about ten structures. Outside of the transition region the number of structures is 2 or less. Notice that with the present counting criterion one dark island on a grey background delivers two structures. In Fig. 21(b), corresponding to a higher noise amplitude $\Delta Y=0.06$, the transition apparent from the equivalent data in Fig. 20(b) (PEEM sequence in Fig. 6) proceeds via formation of about 90 structures. The down burst in the darkness around 3600 s in Fig. 20(b) leads to a spike to 700 in the number of structures in Fig. 21(b). Smaller spikes at later times can be directly connected with darkness down bursts in Fig. 20(b). In an analogous way the number of structures data in Figs. 21(c) and 21(d) can be easily correlated with the darkness data in Figs. 20(c) and 20(d) and from there to the rate data in Fig. 2. The number of

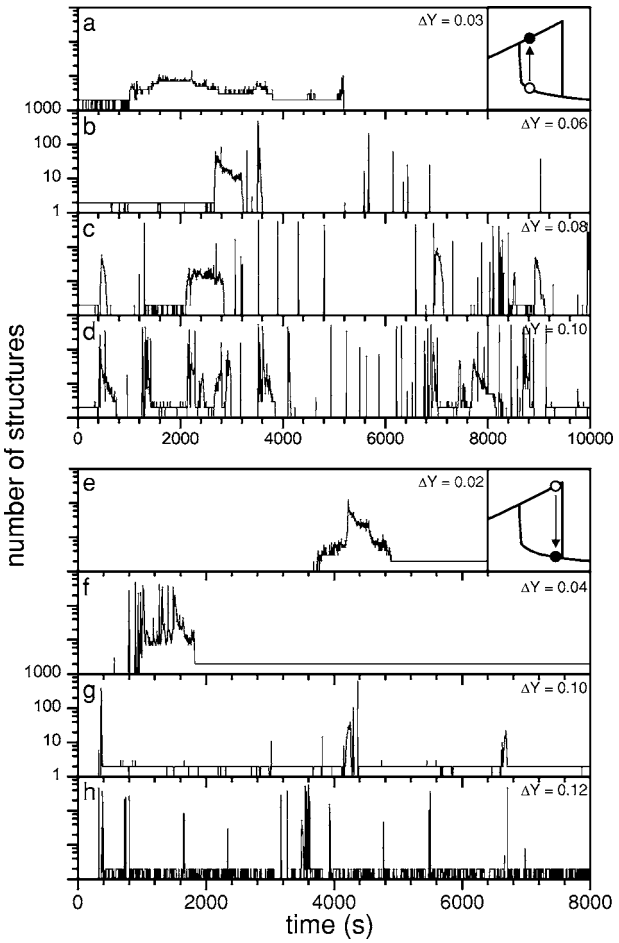

FIG. 21. Logarithmic representation of the number of structures in PEEM patterns (bright and dark patches of any shape) calculated from the pattern sequences whose darkness developments are shown in Fig. 20.

structures data in Figs. 21(e)–21(h), corresponding to the transition between the upper to the lower branch at the right edge of the hysteresis, can be connected in the same way with the darkness data in Figs. 20(e)–20(h) and the rate data in Fig. 2. For example, the relatively calm transition downwards in the darkness curve in Fig. 20(e) is connected with a narrow region in which the number of structures data makes an excursion in Fig. 21(e). Outside of this region the number of structures is fairly small. This type of upper to lower branch transition corresponds to the PEEM pattern sequence in Fig. 11. One finds that the number of structures data in Figs. 21(f)–21(h) correspond in the same way to the darkness data in Figs. 20(f)–20(h) and eventually to the rate data in Fig. 2.

The analysis of the PEEM pictures in terms of darkness and number of structures provides a compact representation of the sequences of PEEM pictures: terabytes of bitmap data are reduced to kilobytes of numbers. However, this reduction by a factor of 10^6 does not reduce the information available from the pictures, it only rules out any significance of a particular picture and extracts the physically significant information in a sequence of PEEM patterns. We conclude that the significant information to be extracted from PEEM patterns measured for the present system are the pattern darkness and the number of structures data. Since these numbers are related to the field of view of the microscope, the more general quantities would be the darkness D and the number of structures N_s in a circular area with a diameter of 270 μm. These numbers are available taking the field of view of the PEEM into account.

The darkness D and number of structures N_s provide complementary information. From the time development of D one obtains information similar to that available from the x-t plots, however, integrated over the whole field of view of the PEEM. The significance of a selected line in the PEEM pictures chosen for construction of the x-t plot is removed since D averages over the whole PEEM pattern. The variation of N_s with time provides detailed informations about the origin of changes of D. If N_s remains at low levels, say, below 10 or so, during a period in which D varies, a transition between the branches of the hysteresis occurs via formation and growth of a few, eventually large islands. For N_s levels which approach 100, many islands are the origin of the transition, and for levels close to 1000 the system makes a transition mediated by a granular island structure. The phenomenology of N_s also provides a close connection to the rate burst and switching phenomena. If N_s exhibits a narrow peak, it indicates that in the darkness D and in the CO_2 rate a burst occurs, if it exhibits an excursion for a longer period, a switch of D and the rate is present.

Without giving explicit examples, it is obvious from the calculated pattern developments in Figs. 15–18 and the corresponding x-t plots that the darkness D and number of structures N_s are also useful quantities for characterizing the processes seen in these data. In contrast to the variations seen in Figs. 20 and 21, the variations of D and N_s do not exhibit the burst and switching phenomena, as already noted earlier.

Although the darkness D is a variable which exhibits a correlation with the coverages of oxygen and CO on the surface, a quantification cannot be given for the experimental PEEM data. The coverage of oxygen atoms on Ir(111) varies between 0 and 0.5, that of CO between 0 and 0.68 [34], however, for the single adsorbate cases only. What the coverages of these species are under reaction conditions is not known, neither is the connection between the brightness (darkness) of a PEEM pattern and these coverages. Accordingly, D is a qualitative, however, very useful quantity. The D values of the patterns obtained by model calculations can be connected quantitatively to the oxygen and CO coverages, since these latter are known at any time during the iteration of the differential Eqs. (1)–(3) and a well defined algorithm connects these coverages to the grey scale used for the patterns display in Figs. 15–18. We refrain from analyzing these connections in detail since not much can be learned from that: the experimental D is, as said, a qualitative measure and, on these grounds, a quantification of the model data D does not provide useful information.

We now turn to the discussion of the connection between the experimental PEEM data and the calculated model data and discriminate for easier identification between experimental (exp) and model (mod) parameters. For the experimental data the following parameters were important.

(1) $Y(=Y_{\mathrm{exp}})$, the CO fraction in the oxygen+CO flux, given by the MFC settings. (2) $\Delta Y(\Delta Y_{\mathrm{exp}})$, the noise ampli-

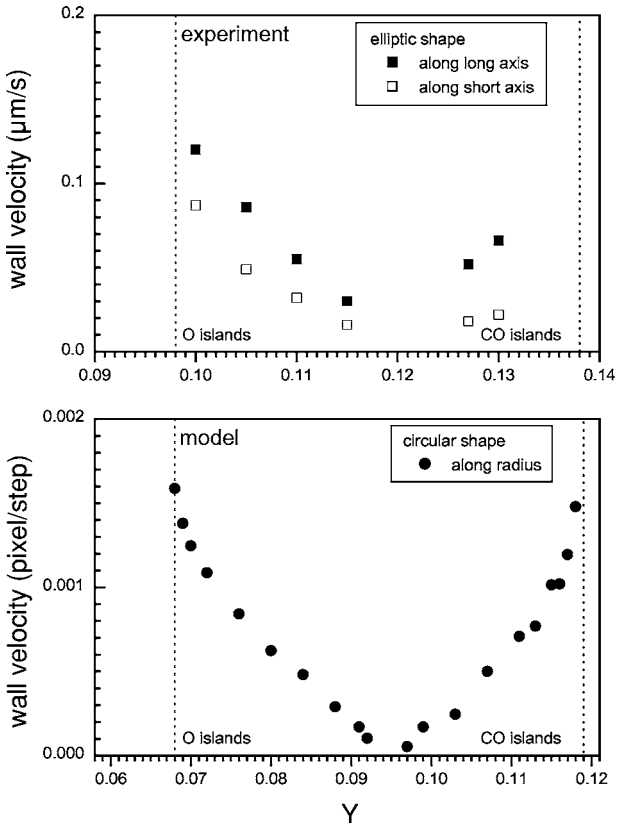

FIG. 22. Wall velocities deduced from measured PEEM (in μm/s) and calculated model (in pixel/step) patterns. The dashed lines provide the positions of the measured and calculated hysteresis borders, respectively.

tude on Y_{exp}; expressed by the variance of a Gaussian distribution, the ΔY values given in the text and figures concerning experimental data, these ΔY values must be divided by 2: $\Delta Y_{exp}=\Delta Y/2$. (3) The time averaging period of noise Δt_{exp}, set at 3 s due to MFC limitations. (4) The space averaging range Δx_{exp}, unknown, must be supplied by surface inhomogeneities.

The respective model parameters are as follows:

(1) $Y(=Y_{mod})$, the CO fraction in the oxygen+CO flux, input value for iterating the PDE. (2) $\Delta Y(\Delta Y_{mod})$, the noise amplitude on Y_{mod}; expressed by the variance of a Gaussian distribution centered at Y_{mod}. (3) The time averaging period of noise Δt_{mod}, set at 9 s at a PDE iteration time step of 0.01 s. (4) The space averaging range Δx_{mod}, equal to the above defined quantity n, and varied between $n=10$ and 100.

The correlations $Y_{exp} \leftrightarrow Y_{mod}$, $\Delta Y_{exp} \leftrightarrow \Delta Y_{mod}$, $\Delta t_{exp} \leftrightarrow \Delta t_{mod}$, and $\Delta x_{exp} \leftrightarrow \Delta x_{mod}$ need to be analyzed in order to judge on the strengths and weaknesses of the model calculations. As noted, Y_{exp} and Y_{mod} for the left and right borders of the hysteresis are different because the position of the model hysteresis was not fitted to the experimental hysteresis by adjusting the parameters which enter the PDEs. This is not a limitation, since we focus on a qualitative comparison between experimental and model data.

The noise amplitudes ΔY_{exp} and ΔY_{mod} refer to the same variance values of the Gaussian noise distributions. However, it must be considered that the relative noise strengths $\Delta Y_{exp}/Y_{exp}$ and $\Delta Y_{mod}/Y_{mod}$ differ because the experimental and model hysteresis are shifted against each other, e.g., the left border of the model hysteresis is located at $Y_{mod}=0.068$, whereas the experimental left border is at $Y_{exp}=0.098$. The smaller value Y_{mod} has the consequence that the accessible range of noise amplitudes ΔY_{mod} is more restricted than the range of the ΔY_{exp} amplitudes. Since the Y values, Y_{exp} as well as Y_{mod}, with superimposed noise have a lower limit of zero, with increasing noise amplitudes ΔY_{exp} and ΔY_{mod} larger fractions of the Gaussian distributed noise components are excluded. In order to prevent a shift of the effective Y values distribution away from the averages Y_{exp} and Y_{mod}, the amplitudes ΔY_{exp} and ΔY_{mod} must be restricted to about half the values Y_{exp} and Y_{mod}. In the present study, this limitation does not affect the experimental PEEM and model pattern data, since these limitations were observed in the selection of noise amplitudes.

The noise averaging times Δt_{exp} and Δt_{mod} were chosen according to the experimental lower limit and a decision made in a previous study, respectively. Other Δt_{mod} values will probably not lead to qualitatively different model pattern developments. It might be that a smaller Δt_{mod} forces higher ΔY_{mod} values to be used in order to reproduce the pattern characteristics. However, this is a minor qualitative aspect which might be studied in detail in the future.

The space averaging ranges Δx_{exp} and Δx_{mod} present the most important aspect. As noted, Δx_{exp} is not under extrinsic control and noise averaging ranges must be supplied by surface inhomogeneities. In the calculations, Δx_{mod} is under control and Figs. 15–18 illustrate that the choice of Δx_{mod}, 10 or 20, has significant effect on the granularity in the pattern development.

Calculations revealed that increasing Δx_{mod} to 50 and 100 leads to a further reduction of the island density, as expected. For more than a qualitative comparison of the experimental and model patterns a length scale which applies to the patterns shown in Figs. 15–18 is required. This scale was obtained by scaling the calculated wall velocities with the experimental values. Figure 22 shows wall velocities deduced by analysis of the experimental PEEM patterns at various Y_{exp} values at small noise amplitudes ΔY_{exp} along the long and short directions of the islands. It is seen that the wall velocity increases upon approaching the border of the hysteresis and is larger in the direction into which the islands are elongated. Close to the left border of the hysteresis the wall velocity in the long direction of the oxygen islands is about 0.15 μm/s. Wall velocities were obtained from model calculations at the left border of the hysteresis and small noise amplitudes ΔY_{mod} irrespective of the noise averaging range Δx_{mod}, as 0.0015 grid points per step. From this we infer that a grid point corresponds to 1 μm, i.e., the 500×500 grid point patterns shown in Figs. 15–18 display a size of 0.5×0.5 mm^2. This value of the model grid fits in the concept of a mesoscale to macroscale for the grid on which the mean-field calculations were performed.

With this size in mind, the low ΔY_{exp} PEEM patterns in Figs. 4, 5, and 10 suggest that the $\Delta x_{mod}=10$ model (left) patterns in Figs. 14 and 16 are appropriate representations of the experimental patterns. A small noise averaging range Δx_{mod} is in line with the assumption that surface inhomoge-

neities are the source of Δx_{exp}. However, a small noise averaging range Δx_{mod} cannot correctly describe the burst and switching phenomena, as was noted earlier based on the results shown in Fig. 19. In order to reproduce burst and switching at high ΔY_{mod} values, at least on the level of parts of the surface, higher Δx_{mod} were needed. There seems to be a correlation between the magnitudes of ΔY_{mod} and Δx_{mod}: in order to reproduce in model calculations the features observed in the experiments, these two quantities must be adjusted with respect to each other. The reason for this requirement is not clear yet.

We emphasize that the suggested correlation between ΔY_{mod} and Δx_{mod} is deduced from calculations in which Δt_{mod} and Y_{mod} were not changed from the values noted above. It is, however, clear that this correlation would be also observed if these latter values are changed within reasonable limits.

VII. CONCLUSIONS

The spatiotemporal development of the CO and oxygen island patterns during the CO oxidation reaction on Ir(111) was studied with PEEM in a 310 μm field of view, in and close to the bistability region of the reaction. In the bistability region the reaction displays a high and low rate branch as a function of the reactant CO (Y) and oxygen ($1-Y$) fractions and constant total reactant gas flux, i.e., a reaction rate hysteresis. With only intrinsic or added small external noise on the CO fraction Y, the transition between the hysteresis branches from the locally stable into the globally stable states close to the hysteresis borders is characterized by very slow nucleation and growth of few and large CO and oxygen islands, respectively. The diameter of these islands is large, >1000 μm, and the velocity of the island walls is small, ~ 0.15 μm/s. With increasing noise amplitude ΔY externally imposed on the Y value, the density of the islands increase at an increasing rate. At sufficiently large ΔY values the state of the surface exhibits bursts from CO rich to oxygen rich and back, as well as switching between CO and oxygen rich and vice versa. These phenomena, recorded on the few 100 μm scale, were previously observed in the CO_2 rate obtained on the 9 mm diameter crystal. Complementary 2D model calculations were performed with a kinetic model which proved sufficient to reproduce the hysteresis phenomenon as well as the consequences of ΔY noise effects on the CO_2 rate. The evolution of calculated 2D CO and oxygen island patterns in a wide Y, ΔY parameter range very well reproduce the measured pattern dynamics. However, the bursts and the switching phenomena at large noise amplitudes on the input gas fractions were not satisfactorily reproduced within the present model.

ACKNOWLEDGMENT

We are indebted to Stefan Karpitschka for developing the pattern recognition and analysis programs.

[1] A. N. Zaikin and A. M. Zhabotinskii, Nature (London) **225**, 535 (1970); H. G. Busse, J. Phys. Chem. **73**, 750 (1969).
[2] R. M. Noyes, R. J. Field, and E. Körös, J. Am. Chem. Soc. **94**, 1394 (1972); R. J. Field, E. Körös, and R. M. Noyes, *ibid.* **94**, 8649 (1972), R. M. Noyes, R. J. Field, H. D. Försterling, E. Körös, and P. Ruoff, J. Phys. Chem. **93**, 270 (1989); A. L. Lin, A. Hagberg, E. Meron, and H. L. Swinney, Phys. Rev. E **69**, 066217 (2004).
[3] Y. Hayase and T. Ohta, Phys. Rev. E **62**, 5998 (2004); T. Ohta, Physica D **151**, 61 (2001).
[4] R. A. FitzHugh, Biophys. J. **1**, 445 (1961).
[5] J. Nagumo, S. Arimoto, and S. Yoshizawa, Proc. IRE **50**, 2061 (1962).
[6] A. H. Hagberg, Ph.D. thesis, University of Arizona, Tucson, 1994.
[7] A. L. Lin, A. Hagberg, A. Ardelea, M. Bertram, H. L. Swinney, and E. Meron, Phys. Rev. E **62**, 3790 (2000).
[8] C. Elphick, A. Hagberg, B. A. Malomed, and E. Meron, Phys. Lett. A **230**, 33 (1997).
[9] P. Grindrod, *The Theory and Applications of Reaction-Diffusion Equations* (Clarendon Press, Oxford, 1996).
[10] A. Hagberg and E. Meron, Phys. Rev. Lett. **72**, 2494 (1994).
[11] A. Hagberg and E. Meron, Phys. Rev. Lett. **91**, 224503 (2003); F. Mertens, N. Gottschalk, M. Bär, M. Eiswirth, A. Mikhailov, and R. Imbihl, Phys. Rev. E **51**, R5193 (1995).
[12] H. H. Rotermund, W. Engel, M. Kordesch, and G. Ertl, Nature (London) **343**, 355 (1990).
[13] G. Ertl, Adv. Catal. **37**, 213 (1990).
[14] R. Imbihl and G. Ertl, Chem. Rev. (Washington, D.C.) **95**, 697 (1995).
[15] R. Imbihl, Prog. Surf. Sci. **44**, 185 (1993).
[16] M. Berdau, G. G. Yelienin, A. Karpowicz, M. Ehsasi, K. Christmann, and J. H. Block, J. Chem. Phys. **110**, 23 (1999).
[17] M. I. Monine, A. Schaak, B. Y. Rubinstein, R. Imbihl, and L. M. Pismen, Catal. Today **70**, 321 (2001).
[18] A. Schaak and R. Imbihl, J. Chem. Phys. **116**, 9021 (2002).
[19] M. Eiswirth, K. Krischer, and G. Ertl, Appl. Phys. A: Solids Surf. **51**, 79 (1990).
[20] J. Hofmann, I. Meusel, J. Hartmann, J. Libuda, and H.-J. Freund, J. Catal. **204**, 378 (2001).
[21] V. Johanek, M. Laurin, A. W. Grant, B. Kasemo, C. R. Henry, and J. Libuda, Science **304**, 1639 (2004).
[22] S. Wehner, F. Baumann, M. Ruckdeschel, and J. Küppers, J. Chem. Phys. **119**, 6823 (2003).
[23] S. Wehner, F. Baumann, and J. Küppers, Chem. Phys. Lett. **370**, 126 (2003).
[24] S. K. Ma, *Modern Theory of Critical Phenomena* (Addison Wesley, Reading, MA, 1976).
[25] M. Baer, Ch. Zülicke, M. Eiswirth, and G. Ertl, J. Chem. Phys. **96**, 8595 (1992).
[26] Y. Hayase, S. Wehner, J. Küppers, and H. R. Brand, Phys. Rev. E **69**, 021609 (2004).
[27] S. Wehner, Y. Hayase, H. R. Brand, and J. Küppers, J. Phys. Chem. B **108**, 14452 (2004).

[28] Y. Hayase, S. Wehner, J. Küppers, and H. R. Brand, Physica D **205**, 15 (2005).
[29] A. S. Mikhailov, *Foundations of Synergetics*, 2nd ed. (Springer, Berlin, 1994), Vol. 1.
[30] S. Wehner, P. Hoffmann, D. Schmeisser, H. R. Brand, and J. Küppers, Phys. Rev. Lett. **95**, 038301 (2005).
[31] P. Hoffmann, R. P. Mikalo, and D. Schmeisser, Solid-State Electron. **44**, 837 (2000).
[32] W. H. Press, S. A. Teukolsky, W. T. Vetterling, and B. P. Flannery, *Numerical Recipes in Fortran* (Cambridge University Press, Cambridge, 1999).
[33] *Physics of Covered Solid Surfaces. Adsorbed Layers on Surfaces*, edited by H. P. Bonzel, Landolt-Börnstein, New Series, Group III (Springer-Verlag, Berlin, 2001), Vol. 42, Subvol. 1, Part 1, pp. 1–58, pp. 455–501, and references therein.
[34] J. Küppers and A. Plagge, J. Vac. Sci. Technol. **13**, 259 (1976).